Case Studies in Construction Materials 21 (2024) e03786

Contents lists available at ScienceDirect

Case Studies in Construction Materials

journal homepage: www.elsevier.com/locate/cscm

Case study

Determining the structural performance of the concrete and masonry shafts in a historic waterway

Baris Gunes [a], Turgay Cosgun [a], Namık Aysal [b], Kamran Samadi [c], Turhan Bilir [a], Onur Şimşek [d], Karsu Hatipoğlu [e], Baris Sayin [a,*]

[a] Department of Civil Engineering, Istanbul University-Cerrahpasa, İstanbul, Türkiye
[b] Department of Geological Engineering, Istanbul University-Cerrahpasa, İstanbul, Türkiye
[c] Institute of Graduate Sciences, Istanbul University-Cerrahpasa, İstanbul, Türkiye
[d] Fatih Sultan Mehmet Vakıf University, Kuram, İstanbul, Türkiye
[e] İstanbul Water and Sewerage Administration, İstanbul, Türkiye

ARTICLE INFO

Keywords:
Concrete shaft
Vertical shaft
Seismic performance
Water supply system
Historical buildings

ABSTRACT

Determining the seismic performance level of shaft structures is crucial due to their vital role in ensuring a water supply. Since these are underground structures, the loads they encounter and the structural modeling processes differ significantly from those of above-ground structures. Accordingly, the primary aim of this paper is to introduce a new modeling methodology for the seismic performance assessment of shaft structures, considering all relevant parameters. This unique approach also incorporates pertinent sections from various applicable local seismic codes. For this purpose, a total of 15 shaft structures located on the historic Atik Valide Waterway, constructed in 1583, were examined. To create numerical models of the shafts, soil exploration parameters were utilized, and the shaft surface-soil interaction was represented by nonlinear p-y springs. An integral part of the presented methodology involved segmenting the shafts at regular intervals, with each segment defined as a separate story. The analysis results demonstrated that the modeling methodology is accurate and aligns well with the observed conditions of the shafts. Considering the significant risk of extensive damage to sewerage systems in urban areas due to soil liquefaction during seismic events, this study is anticipated to serve as a valuable reference in the literature by introducing a new, accurate methodology for identifying potential seismic risks.

1. Introduction

Throughout history, humans have constructed various structures to utilize water, a fundamental requirement for life. Structures such as cisterns, wells, and waterways were designed to facilitate the use of water for vital needs. Water is a fundamental source of life and has always been one of the most critical needs for every settled society. Many civilizations were established near water sources. Although the settlements were located next to a flowing or stagnant water body, it has always been necessary to construct various structures to collect, distribute, and utilize water. Furthermore, new water structures were required for the transportation and storage of water in cases where settlements needed to be established at a distance from the water source due to security concerns or other reasons, or when water availability was insufficient [1].

* Corresponding author.
E-mail address: barsayin@iuc.edu.tr (B. Sayin).

https://doi.org/10.1016/j.cscm.2024.e03786
Received 16 April 2024; Received in revised form 28 July 2024; Accepted 20 September 2024
Available online 9 October 2024

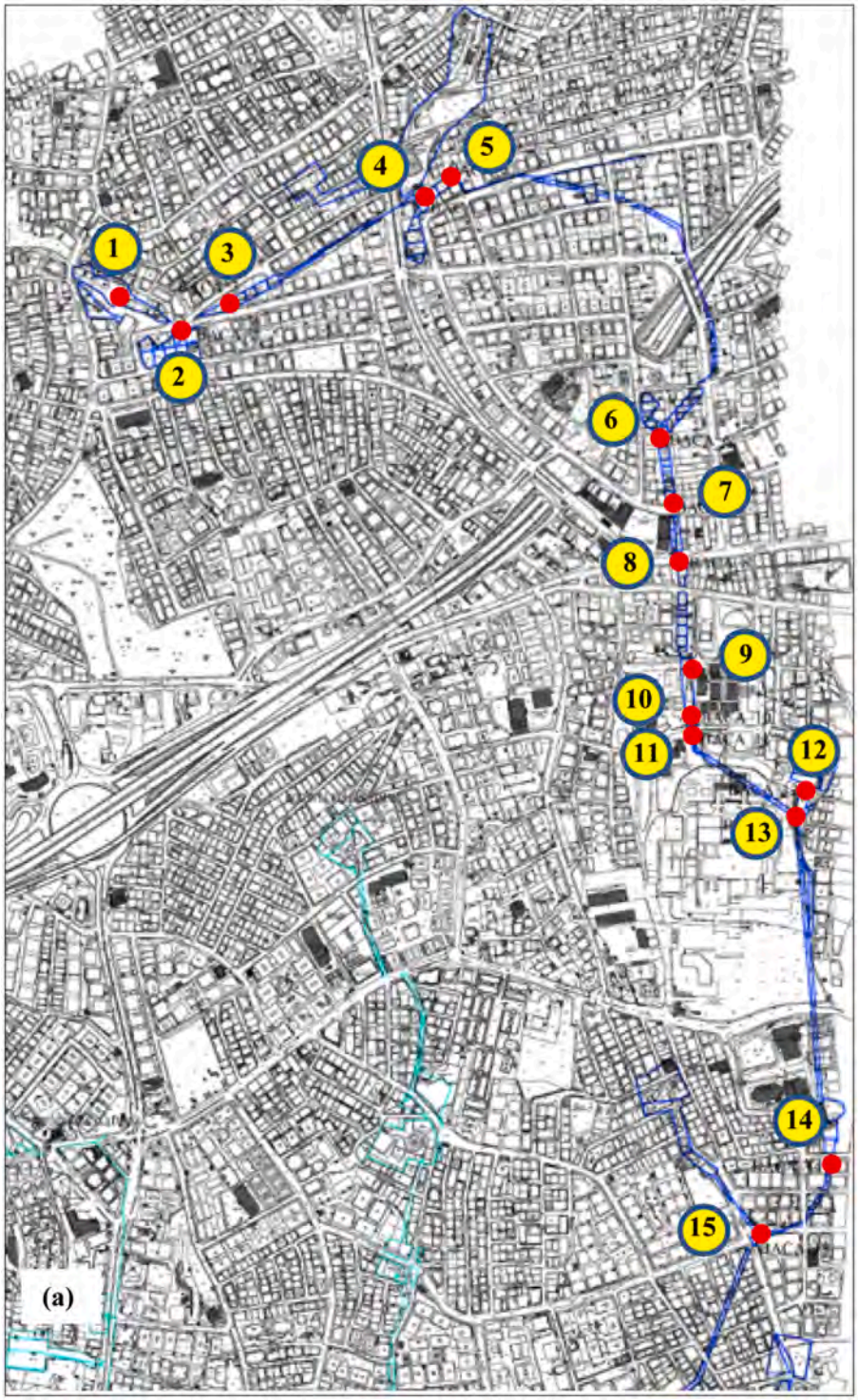

Fig. 1. (a) Waterway line (blue) and 15 shafts (red circles) placed along this line.

The history of waterways in Istanbul dates back to the reign of Emperor Hadrian (117–138 AD), during which the first major water transmission system, including extensive multi-story aqueducts, was constructed in the 4th century. However, no new aqueducts were added during the Byzantine period, and even the existing ones were not properly maintained. Consequently, the Roman waterways were known to be unusable by the 15th century [2]. The Ottoman state not only restored and reactivated the long-abandoned transmission lines and facilities constructed in ancient times but also enhanced them according to its own principles. Unlike the

Fig. 2. . Photos of the examined shafts.

Byzantine reliance on cisterns, the Ottoman approach to constructing waterways prioritized the continuous flow of water, reflecting their belief that "flowing water is pure." This shift in methodology marked a significant departure from previous practices [3]. Another important detail was in Ottoman water structures, emphasis was placed on social benefit rather than on features designed solely for pleasure and enjoyment. The pools designed to comfort patients at *Darüşşifa* (hospital) and the *shadirvan* (public fountain unit) pool in Bursa Ulucami Mosque are well-known examples of such structures with known public functions. In Istanbul, the construction of the

Table 1
Geometric properties of the shafts.

Shaft no	Depth (m)	Geometry	Diameter / section size (cm)	Wall thickness (cm)
1	9.35	Circular	117	11
2	9.72	Rectangular	80 × 72	-
3	*1.36*	*Does not have a regular geometry. Constructed using bricks and briquettes.*		
4	6.28	Rectangular	95 × 97	13, 15, 16, 21
5	3.47		95 × 95	13
6	10.20		98 × 99	-
7	12.57		96 × 98	17, 19, 17, 17
8	12.53		70 × 72	5
9	8.61		100 × 102	21, 21, 23, 21
10	7.05		126 × 118	15, 6, 8, 6
11	4.15	Circular	81	10
12	2.27	Rectangular	96 × 102	21, 18, 22, 19
13	1.27		136 × 145	17, 20, 18, 17
14	1.02		98 × 100	21, 19, 21, 18
15	2.14		69 × 71	5

Table 2
Soil and earthquake parameters.

Shaft no	Local Soil Class	γ (kN/m^3)	V_s (m/s)	ϕ°	Soil type	Horizontal bedding coefficient (MN/m^3)	DD-3 S_s, S_1 (g)	DD-2 S_s, S_1 (g)	DD-3 PGA (g)	DD-2 PGA (g)
1	ZB	24	800	38	Quartzite	450	0.337 0.096	0.839 0.234	0.145	0.345
2	ZB	24	800	38		500	0.338 0.096	0.839 0.234	0.145	0.346
3	ZB	24	800	38		300	0.337 0.096	0.837 0.234	0.145	0.345
4	ZC	20	400	34	Dyke	150	0.335 0.095	0.828 0.232	0.144	0.341
5	ZC	20	400	34		100	0.334 0.095	0.827 0.232	0.144	0.341
6	ZC	20	400	34		250	0.337 0.096	0.837 0.234	0.145	0.345
7	ZB	24	1000	40	Limestone 1	700	0.338 0.096	0.839 0.234	0.145	0.346
8	ZB	24	1000	40		700	0.339 0.096	0.840 0.235	0.146	0.346
9	ZB	24	1000	40		600	0.340 0.096	0.844 0.235	0.146	0.348
10	ZB	24	1000	40		520	0.341 0.097	0.844 0.235	0.146	0.348
11	ZB	24	1000	40		420	0.341 0.097	0.846 0.236	0.147	0.348
12	ZB	24	1000	40		380	0.342 0.097	0.846 0.236	0.147	0.349
13	ZA	26.5	1500	43	Limestone 2	540	0.342 0.097	0.849 0.236	0.147	0.349
14	ZA	26.5	1500	43		540	0.347 0.098	0.859 0.239	0.147	0.349
15	ZA	26.5	1500	43		540	0.348 0.098	0.860 0.239	0.149	0.354

* γ= unit weight of soil, V_s= shear wave speed, ϕ°= internal angle of friction of soil, DD-3= frequent earthquake with a 50 % probability of exceedance in 50 years and a recurrence interval of 72 years, DD-2= standard earthquake with a 10 % probability of exceedance in 475 years and a recurrence interval of 72 years, DD-1= major earthquake with a 2 % probability of exceedance in 2475 years and a recurrence interval of 72 years, ZA, ZB, ZC: Local soil classes, ZA: Solid hard rocks, ZB: Slightly weathered rocks of medium strength, ZC: Moderately compact sand and gravel or very solid clay layers, S_s: short period mapped spectral acceleration parameter S_1: mapped spectral-acceleration at period of 1.0 s

first Ottoman-era waterway system commenced in 1453, setting the groundwork for the development of a complex network consisting of 16 independent waterways, which was completed in 1755. Mehmed II (Mehmed the Conqueror) initially focused on repairing the galleries of the Roman waterway that ran from the Belgrade Forests between *Cebeciköy* and the Aqueduct of Valens. Additionally, Mehmed II oversaw the complete reconstruction of 22 aqueducts that had fallen into disrepair. He also directed the row of aqueducts on the Golden Horn side of the Aqueduct of Valens to supply water to fountains, which were subsequently named '*Kırkçeşme*' meaning forty fountains. During the reign of Suleiman the Magnificent, Sinan the Architect constructed several facilities including the Maglova aqueduct and Güzelcekemer (aqueduct) over the Kâğıthane stream, from 1554 to 1563. These additions connected the stream to the

Table 3
Mechanical properties of the concrete used in shafts.

Shaft no	Material	γ (kN/m^3)*	f_k (MPa)*	f_{vko} (MPa)*	E (MPa)*
1	Concrete	25	10	0.7	15811
2	Concrete	25	10	0.7	15811
	Brick	11	2.8	0.1	2000
3	Brick	11	2.8	0.1	2000
4	Concrete	25	10	0.2	15811
5	Concrete	25	10	0.7	15811
6	Concrete	25	10	0.7	15811
	Stone	25	2	0.7	1500
7	Concrete	25	10	0.7	15811
	Rock	25	4.6	0.7	15811
8	Concrete	25	10	0.7	15811
	Rock	25	4.6	0.7	15811
9	Concrete	25	10	0.7	15811
	Stone	25	2	0.7	1500
10	Concrete	25	10	0.7	15811
11	Concrete	25	10	0.7	15811
12	Concrete	25	10	0.7	15811
13	Concrete	25	10	0.7	15811
14	Concrete	25	10	0.7	15811
15	Concrete	25	10	0.7	15811

* γ= unit weight of shaft wall, f_k= Characteristic compressive strength of the shaft wall, f_{vko}=shear strength of the shaft wall, E=Young modulus

Table 4
Load combinations.

Combination	ID	Definition
1	D_01a_L	Dead Load + Ground/Surcharge Load (Rest)
2	D_05a_Exp	Dead Load + Ground/Surcharge Load (active) + Earthquake Load (Ex+0.3Ey)*
3	D_05a_Eyp	Dead Load + Ground/Surcharge Load (active) + Earthquake Load (Ey+0.3Ex)*

* Ex+0.3Ey: represents the combination of full earthquake load in the x-direction and 30 % of the earthquake load in the y-direction. Ey+0.3Ex: represents the combination of full earthquake load in the y-direction and 30 % of the earthquake load in the x-direction.

Fatih-era Kırkçeşme line in Cebeciköy. As a result, the longstanding water issue within the walled city of Istanbul was finally resolved, providing the city with a daily supply of 12,000 m^3 of water. This 55 km long line supplied water to 580 fountains [4]. Additionally, on the Anatolian side, particularly in Üsküdar, the Üsküdar Waterways were constructed between 1547 and 1874, consisting of 17 independent foundation water lines. One Among these waterways is the *Atik Valide* (also known as *Nurbanu Sultan*) Waterway. The waterway structures in Ottoman architecture include break pressure tanks, drain gratings, pools, and dykes for water collection; galleries, chimneys, aqueducts, and water towers for water transmission; as well as water tanks and distribution chambers for distributing water throughout the city. Üsküdar in Istanbul relied on wells and cisterns for water supply from 1352, when the Ottomans took control, until 1547 when the Mihrimah Sultan waterway was completed. During the Ottoman period, a total of 35 transmission lines, comprising 18 large and 17 small ones, were built in Üsküdar. Among these, the Atik Valide and Ibrahim Pasha waterways stand out as the largest both in terms of flow rate and length. The length of the "Atik Vâlide" waterway, constructed by Nurbanu Valide Sultan (the wife of Selim II), is 153,000 m with a flow rate of 676 m^3/day; whereas, the Damat Ibrahim Pasha waterway measures 146, 000 m in length with a flow rate of 448 m^3/day [5].

During earthquakes, tall structures such as ventilation and maintenance shafts in water systems experience strong shaking forces that can potentially cause structural damage or collapse. Therefore, conducting a comprehensive seismic assessment of these structures is crucial to ensure their resilience and safety. Consequently, numerous researchers have studied shaft structures, with a particular focus on lateral soil pressure and seismic behavior. In one such study, Kim et al. [6] investigated lateral soil pressure on a vertical circular shaft through experimental studies and theoretical analysis. Their findings indicated that the magnitude and distribution of lateral soil pressure were not strictly linearly correlated with excavation depth. Instead, they observed that the lateral earth pressure acting on the vertical circular shaft decreases by up to 80 % at certain depths. Consequently, they argued that the commonly used Rankine equation often overestimates lateral pressure. Chen and Zhang [7] investigated the seismic response of vertical shafts on soft grounds. They found that the shaft mostly acts as a rigid body during a ground motion. The maximum bending moment in the vertical direction was observed at the bottom of the shaft, whereas, the transverse axial force was found to occur at about 2/3 depth of the shaft. Faustin et al. [8] created a small-scale test model in a geotechnical centrifuge to simulate shaft excavation in clay. Their results revealed that the majority of the horizontal soil stress acting on the circular shaft is transformed into hoop stresses with minimum bending stress in the shaft lining, and the hoop stresses gradually increase as the excavation deep increases. Chen and Jia [9] examined the impact of soil loss on the static and seismic behavior of shafts. Their findings indicated that soil loss may change the static and seismic behavior of shafts through increasing bending moments and decreasing axial pressures. Zhang and Chen [10] introduced a nominal flexibility ratio formula to examine seismic behaviors of deep shafts based on the quasi-static approach. The authors employed

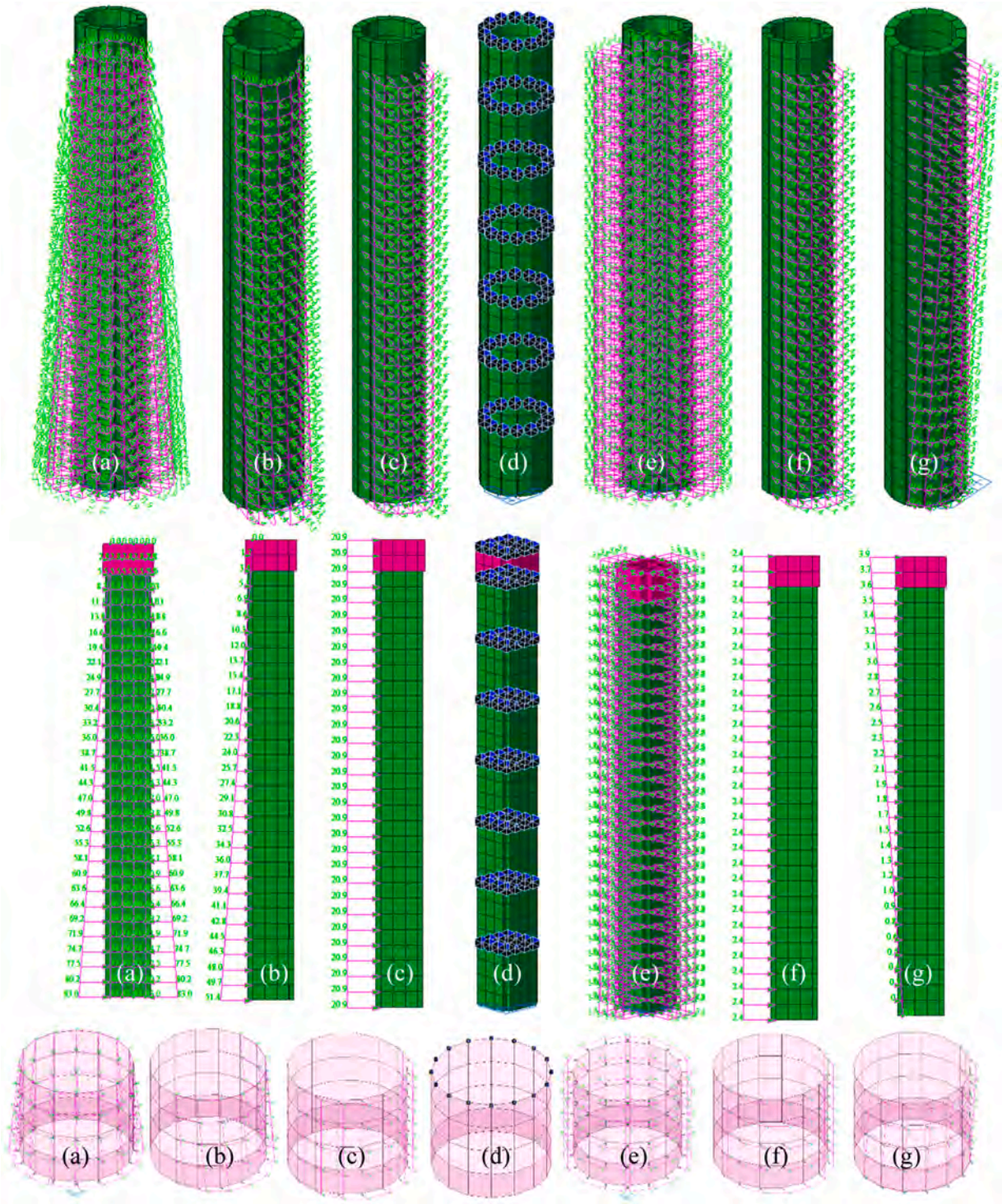

Fig. 3. Shafts 01–03 (under DD-2 earthquake conditions): a) lateral effect of the embankment load at rest, b) active soil load in the x direction, c) seismic load of the soil in the x direction, d) seismic load of the ground in the x direction, e) lateral effect of the surcharge load at rest, f) active surcharge load in the x-y directions, g) seismic load of the surcharge in the x-y directions.

three-dimensional dynamic time history analyses to verify the results. Their findings revealed that the distribution pattern of internal forces and deformation modes in the shafts is primarily influenced by the depth-to-width ratio rather than the inner-to-outer diameter ratio. Additionally, they found that the magnitude of internal forces is affected by the inner-to-outer diameter ratio when considering

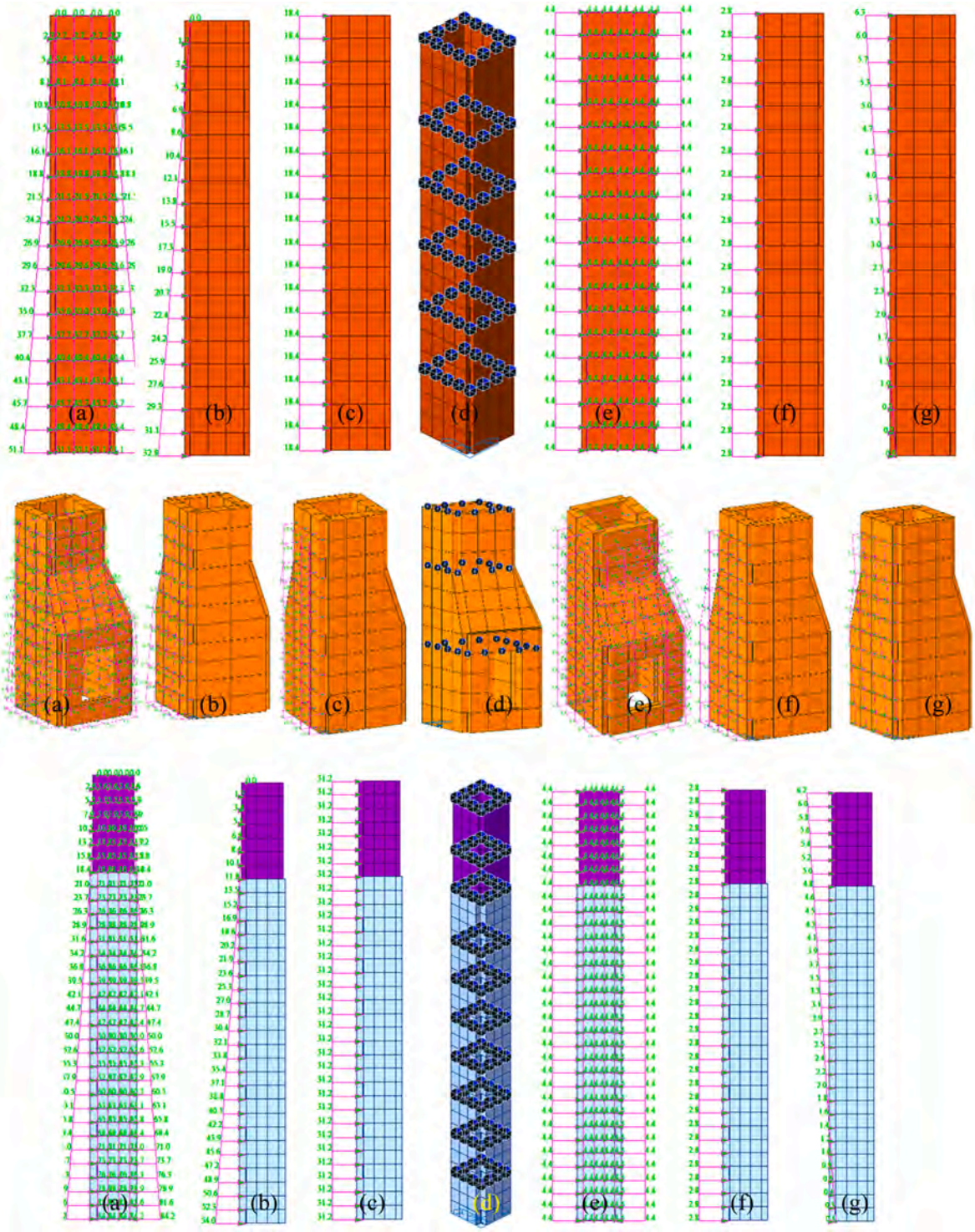

Fig. 4. Shafts 04–06 (under DD-2 earthquake conditions): a) lateral effect of the embankment load at rest, b) active soil load in the x direction, c) seismic load of the soil in the x direction, d) seismic load of the ground in the x direction, e) lateral effect of the surcharge load at rest, f) active surcharge load in the x-y directions, g) seismic load of the surcharge in the x-y directions.

the same shaft depth-to-width ratio and surrounding soil condition. Zhanga et al. [11] developed an analytical solution to examine the dynamic responses of a vertical shaft located in a shaft-tunnel junction. Their results suggested that if the shaft is subjected to transverse dynamic loads above the ground surface, the displacements of the shaft may be reduced; on the other hand, if the

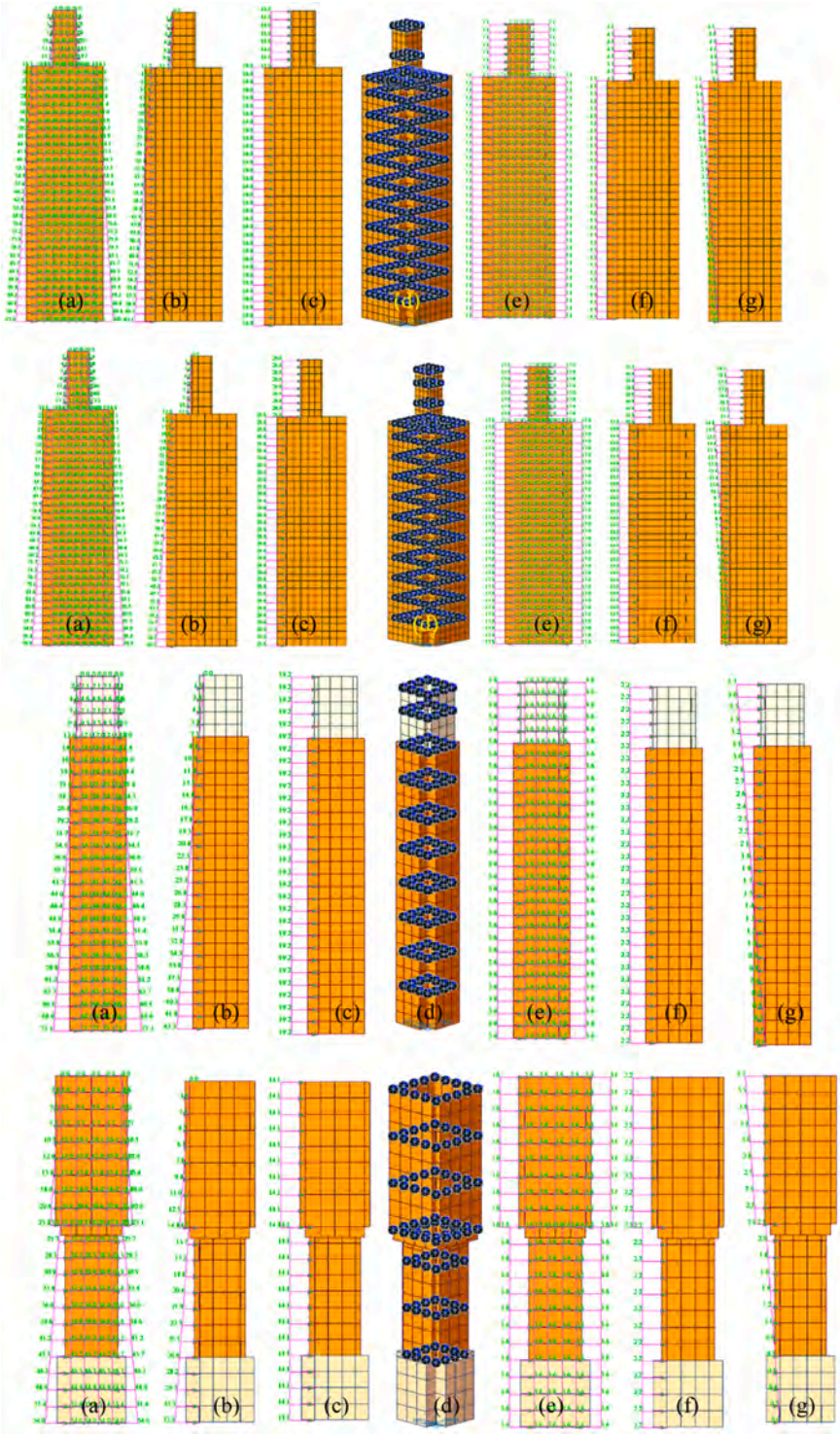

Fig. 5. Shafts 07–10 (under DD-2 earthquake conditions): a) lateral effect of the embankment load at rest, b) active soil load in the x direction, c) seismic load of the soil in the x direction, d) seismic load of the ground in the x direction, e) lateral effect of the surcharge load at rest, f) active surcharge load in the x-y directions, g) seismic load of the surcharge in the x-y directions.

shaft-tunnel junction is subjected to transverse seismic impacts, the effect of the tunnel might be negligible. Kwon and Yoo [12] examined the dynamic behavior of a vertical tunnel shaft during liquefaction. Their findings suggested that as the earthquake magnitude and shaft depth increase, the shaft will be subjected to a greater kinematic force due to liquefaction. Zhang et al. [13]

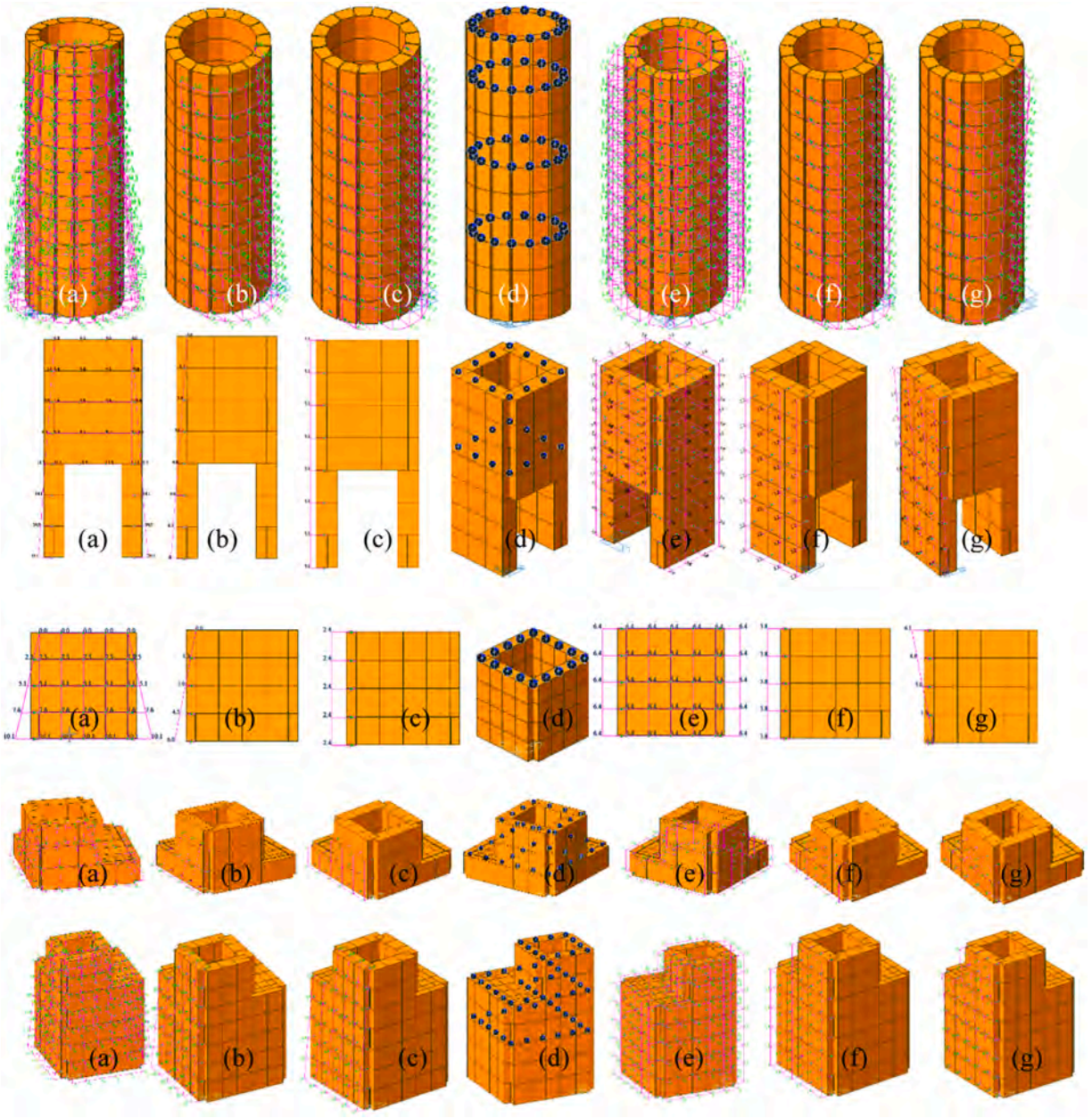

Fig. 6. Shafts 11–15 (under DD-2 earthquake conditions): a) lateral effect of the embankment load at rest, b) active soil load in the x direction, c) seismic load of the soil in the x direction, d) seismic load of the ground in the x direction, e) lateral effect of the surcharge load at rest, f) active surcharge load in the x-y directions, g) seismic load of the surcharge in the x-y directions.

proposed a mechanical model to examine the seismic response of a vertical shaft with double linings based on elastic foundation beam theory. The authors simplified shaft linings as parallel Euler Bernoulli beams and used uniformly distributed springs to represent their interactions. The agreement between the analytical solution and the finite element analysis outcomes indicated that the maximum horizontal displacement of the inner lining exceeds that of the outer liner. Additionally, the relative stiffness between the linings plays a significant role in determining the maximum bending moment on the inner lining. Li et al. [14] examined the mechanical behaviors of shaft lining failures and prevention methods by taking temperature stress, soil pressure, self-weight stress, and draining additional force into account. Their results showed that the primary failure mode of shaft linings is shear failure. Furthermore, the authors suggested grouting reinforcement, shaft lining coating with composite new materials, and unloading secondary lining methods for preventing shaft failures.

Kim et al. [15] explored the lateral earth pressure acting on vertical circular shafts, focusing on its magnitude and distribution in weathered soil with considering the three-dimensional arching effect. The authors propose a novel theoretical approach for estimating

Table 5
Performance based structural analysis/design and evaluation methods.

Parameter	Value / Class
Intended use of Structures	Waterway shafts
ERMGHB 2017 Importance Factor	Local
Earthquake Ground Motion Level	DD−2, DD−3
Target Performance	Controlled Damage, CD*
Analysis/design method	Strength-Based Design, SBD
Analysis/Design Method Applied in Global Earthquake under TTEC−2020	Type A

* *Controlled damage* is a performance target, which corresponds to damage that is not too severe and is mostly repairable to the structural system elements of the building, ensuring life safety.

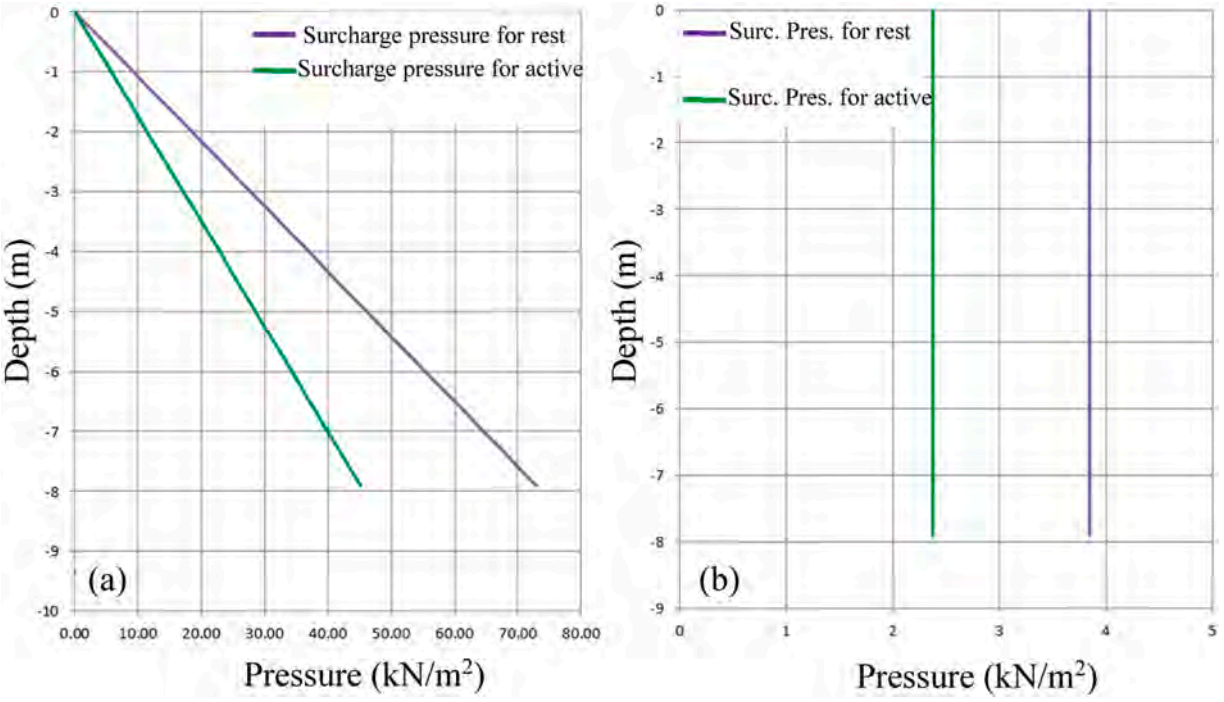

Fig. 7. (a) Lateral soil pressure (b) Surcharge pressure.

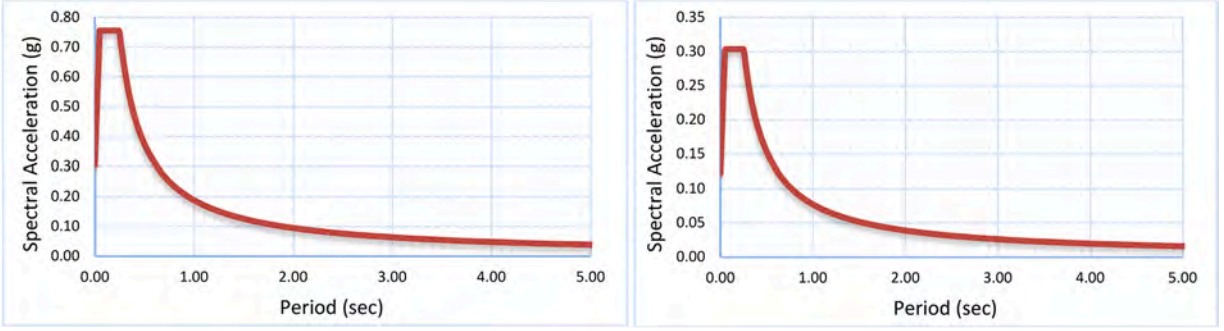

Fig. 8. Response spectrums for DD-2 (left) and DD-3 (right) Earthquake Ground Motions.

earth pressure in multi-layered c–φ soils and validate their findings through comparisons with centrifuge and full-scale field tests. Their study introduced some insights into soil-structure interaction and enhances design methodologies for vertical shafts in geotechnical engineering applications. Qiao et al. [16] conducted an in-depth examination of deformation monitoring data from a very deep circular shaft excavation in China. First, the authors reviewed the shaft project and the geological parameters around. They conducted statistical analyses to compare these findings with similar excavations and explore the relationships between horizontal and vertical

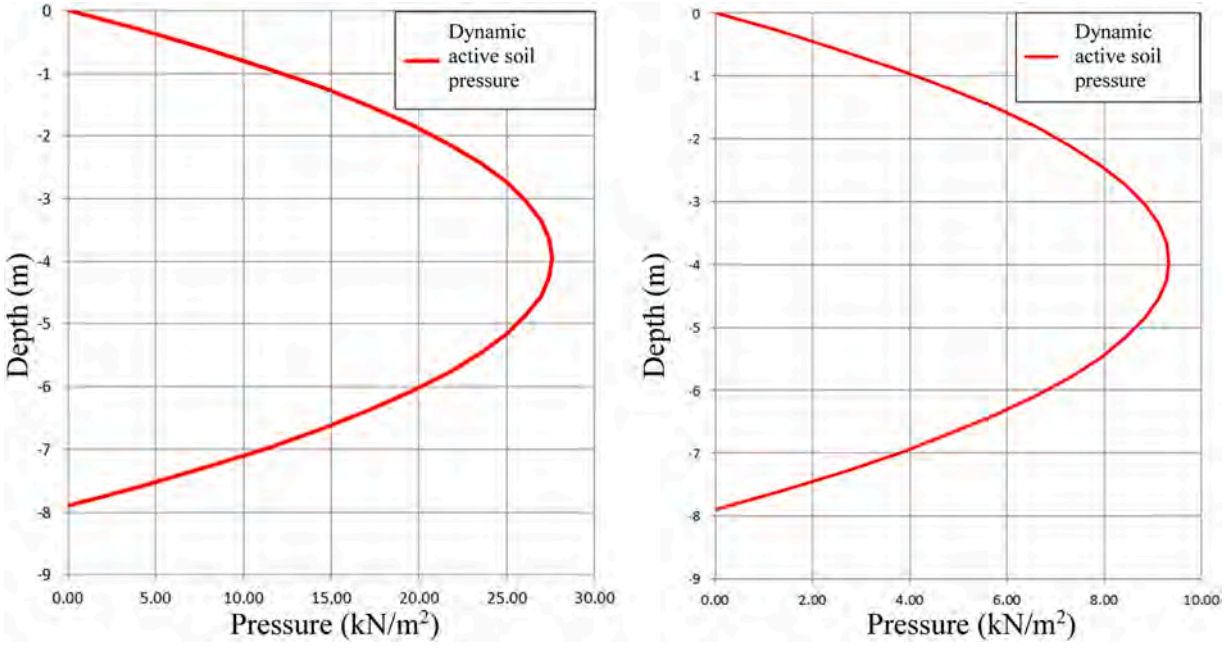

Fig. 9. Earthquake-Induced Soil Pressures for DD-2 (left) and DD-3 (right) Earthquake Ground Motions.

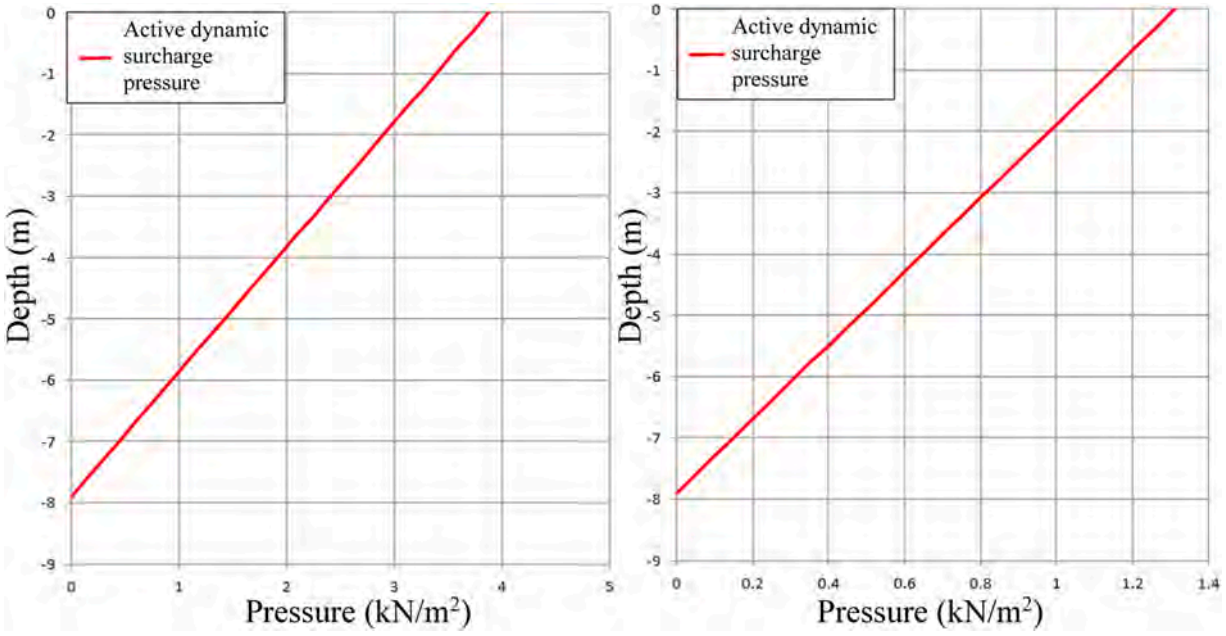

Fig. 10. Earthquake-Induced Surcharge Pressures for DD-2 (left) and DD-3 (right) Earthquake Ground Motions.

deformations. Their study concluded with a discussion on the overall deformation mechanism of the shaft, presenting insights into its structural behavior under specific geological conditions. Chehadeh et al. [17] conducted parametric numerical analyses to reveal the interaction between vertical circular shafts and surrounding soil. Utilizing ABAQUS, the researchers employed three-dimensional nonlinear finite-element methods considering elasto-plastic soil behavior with the Mohr–Coulomb failure criterion for retained soil and nonlinear soil-shaft interface conditions. They explored practical aspects of shaft design, including earth pressure distribution assumptions, horizontal arching mechanisms, the influence of wall deformations on earth pressures, three-dimensional surcharge pressure distribution on circular walls, and the effects of shaft radius and soil type. Mahmoodi et al. [18] employed the distributed dislocation approach to analyze the distributed shear interaction functions (DSIFs) and torsional rigidity of radially cracked circular

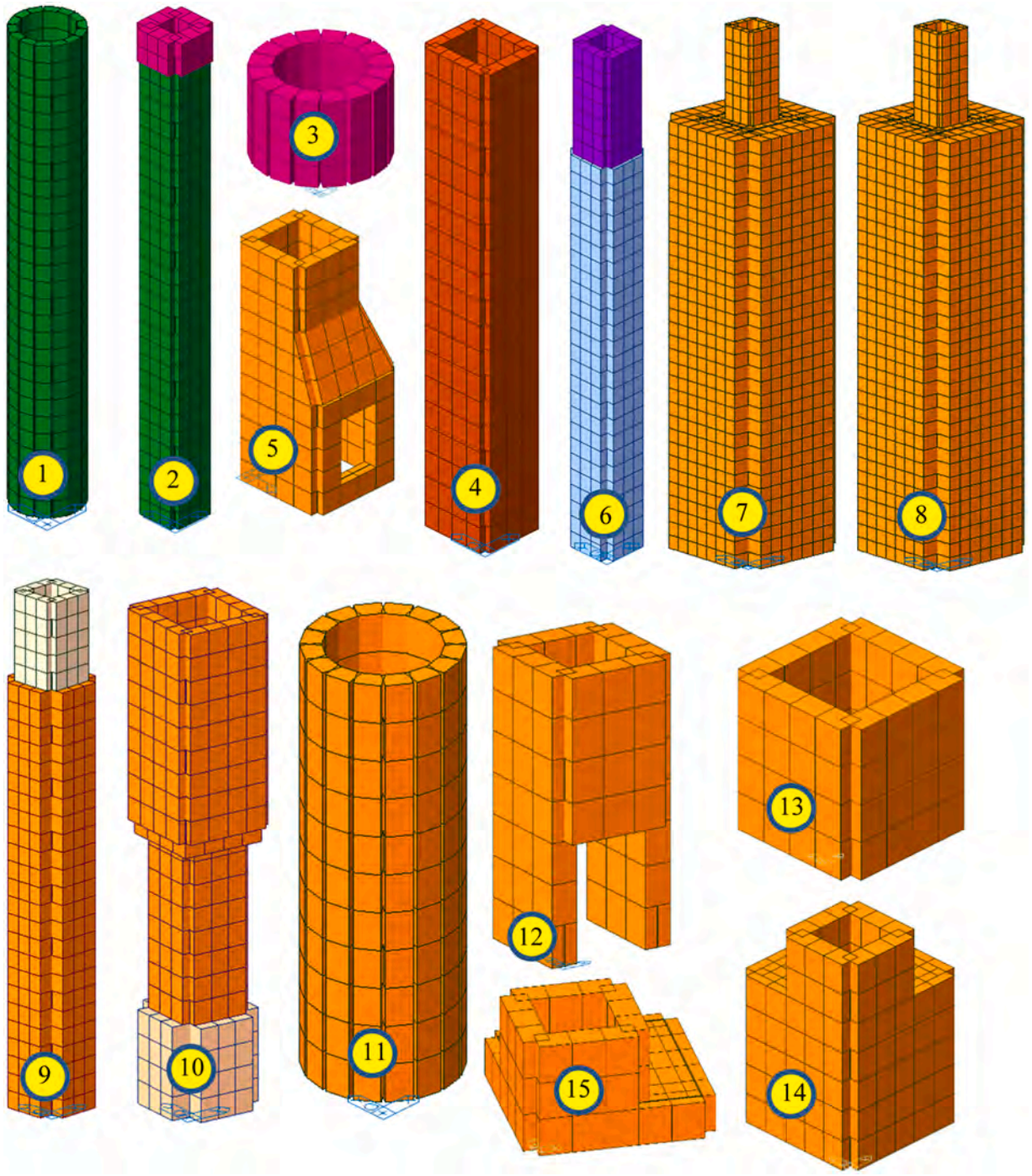

Fig. 11. 3D finite element models of the shafts.

bars with an FG coating layer under transient torsional loading. Their study focuses on radial cracks extending throughout the circular bars. Cho et al. [19] examined lateral earth pressure magnitude and distribution around a vertical circular shaft during excavation. The authors conducted centrifuge model tests and finite element analyses, performing comprehensive parametric studies to evaluate various design factors. The numerical results were validated against experimental measurements to ensure accuracy. Chehadeh et al. [20] conducted parametric numerical analyses to examine interaction between vertical circular shafts and surrounding soil, focusing on shafts with holes in the walls. The authors utilized three-dimensional nonlinear finite element analyses with ABAQUS, incorporating elasto-plastic soil behavior for the retained soil and a non-linear soil-shaft interface to simulate realistic soil-structure interactions

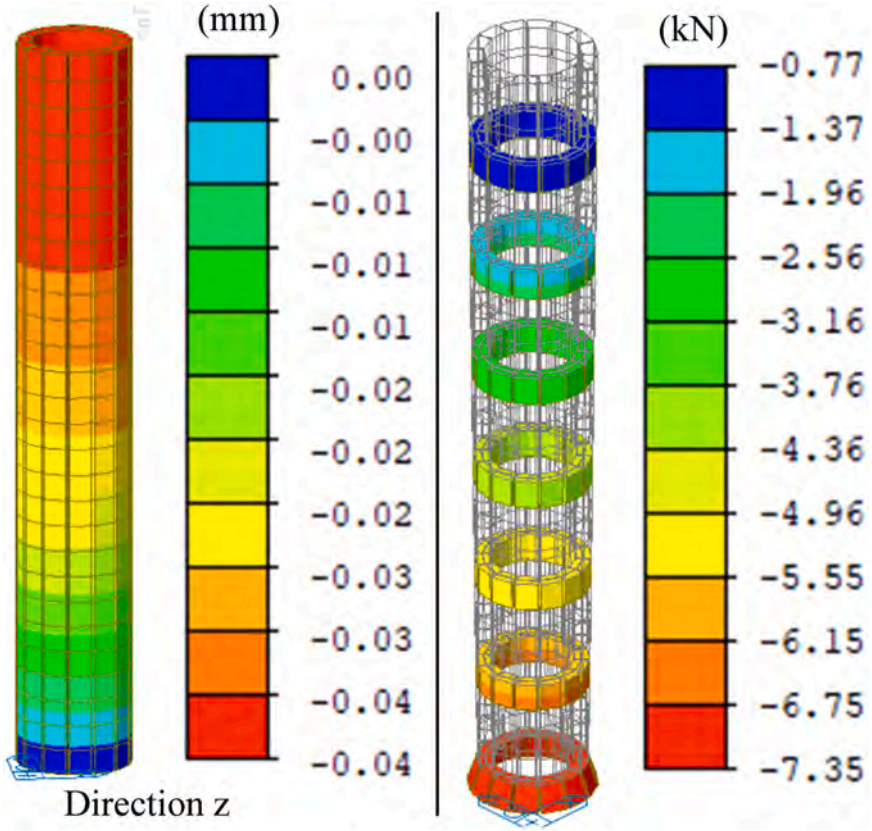

Fig. 12. Displacements and axial forces resulting from vertical loads for the Shaft 01.

Preserving historical and cultural heritage and ensuring its continuity into the future is valuable, particularly for buildings that are no longer constructed today. It is important that such buildings have adequate resistance against the environmental and structural effects they encounter, as they serve as tangible representations of the construction techniques of the periods in which they were erected. On the other hand, presenting practical and accurate assessment and modeling approaches for underground structures would make a valuable contribution to the existing literature. Accordingly, the current study presents a comprehensive modeling methodology for seismic performance analyses of the shafts within the historic Atik Vâlide waterway in Istanbul. Since these shaft structures are historical, the local code, Earthquake Risk Management Guide for Historical Buildings (ERMGHB 2017) [21], was consulted to determine the target performance and design approach. Additionally, as shafts are underground structures, the Turkish Highways and Railways Tunnels and Other Ground Structures Earthquake Code (TTEC 2020) [22] and the Turkish Building Earthquake Code (TBEC 2018) [23] were also utilized. Although the structures are regarded as having 'Local' significance, the typical target performance of Controlled Damage for Earthquake Ground Motion Levels DD-2 and DD-3 was considered. The assessment/design approach was established as Strength-Based Design (SBD). Therefore, a unique methodology was applied by combining relevant sections from various applicable codes. Considering the susceptibility of urban sewage systems to earthquake-induced damage, particularly from soil liquefaction, this study is expected to make a valuable contribution to the literature by presenting an effective methodology for assessing the seismic resilience of such structures.

2. The examined structure

Numerical analyses were conducted for the 15 shafts in the Atik Valide Water System. This system, as extensively described in the introduction, was constructed in 1583 to supply water to the madrasahs (Islamic schools), baths, and other charitable institutions affiliated with the Atik Valide Mosque and Complex in Üsküdar, Istanbul. Figs. 1 and 2 shows the waterway line where these shafts are located, with images of the shaft structures. These shafts serve as architectural features that allow workers to access underground water channels for repair and maintenance purposes. Shafts, also utilized in aqueducts and dykes, are structures large enough for a person to enter, spaced approximately 50 m apart along the entire length of the waterway lines. The entrances to the shafts were constructed approximately 60–70 cm above the soil level.

Tables 1–3 present the geometric properties of the shafts, soil and earthquake parameters, and mechanical properties of the concrete used in shafts, respectively. The soil structure along the height of each shaft typically has a single soil profile and type. The examined shafts are relatively low in height; therefore, a single soil profile is considered for each shaft.

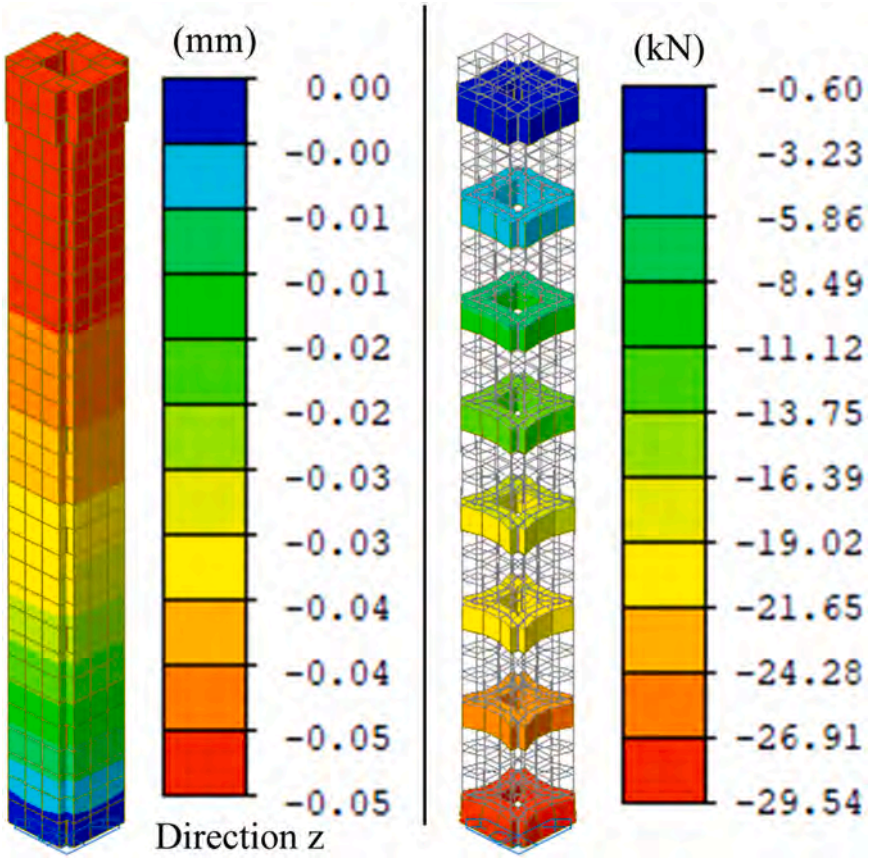

Fig. 13. Displacements and axial forces resulting from vertical loads for the Shaft 02.

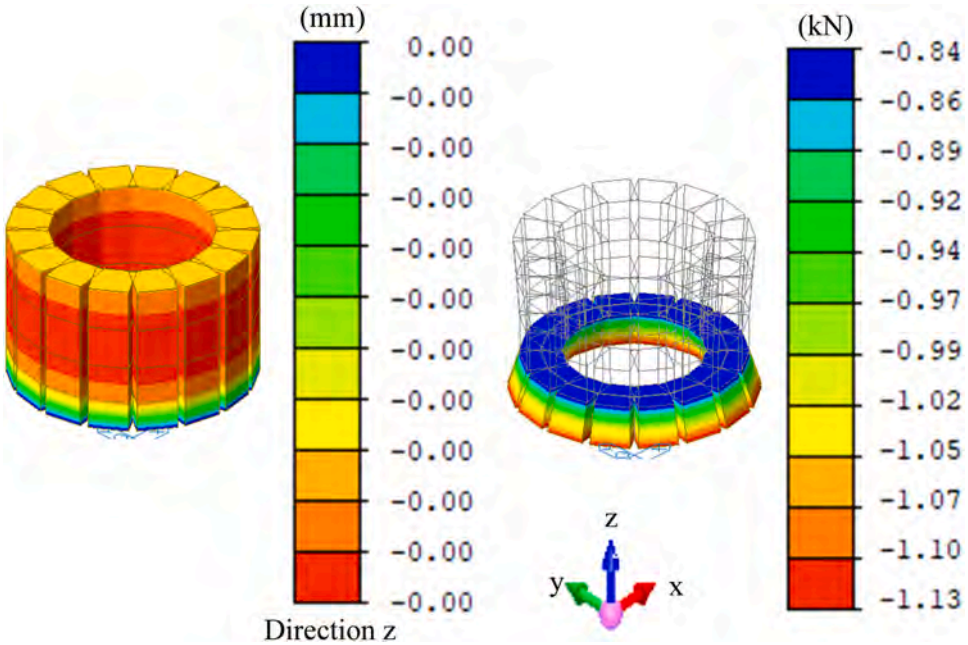

Fig. 14. Displacements and axial forces resulting from vertical loads for the Shaft 03.

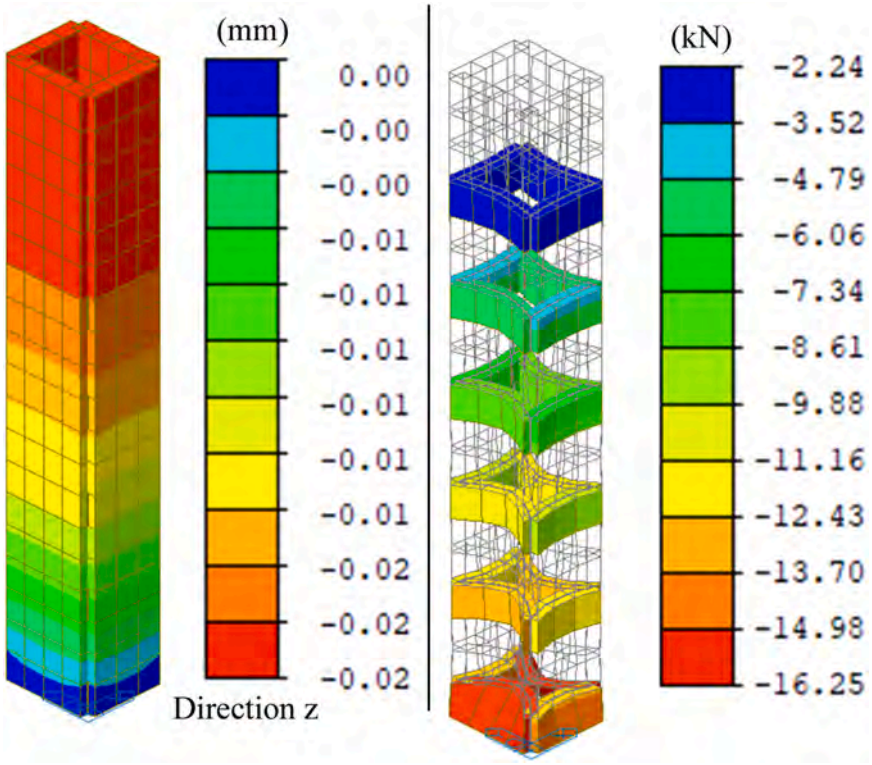

Fig. 15. Displacements and axial forces resulting from vertical loads for the Shaft 04.

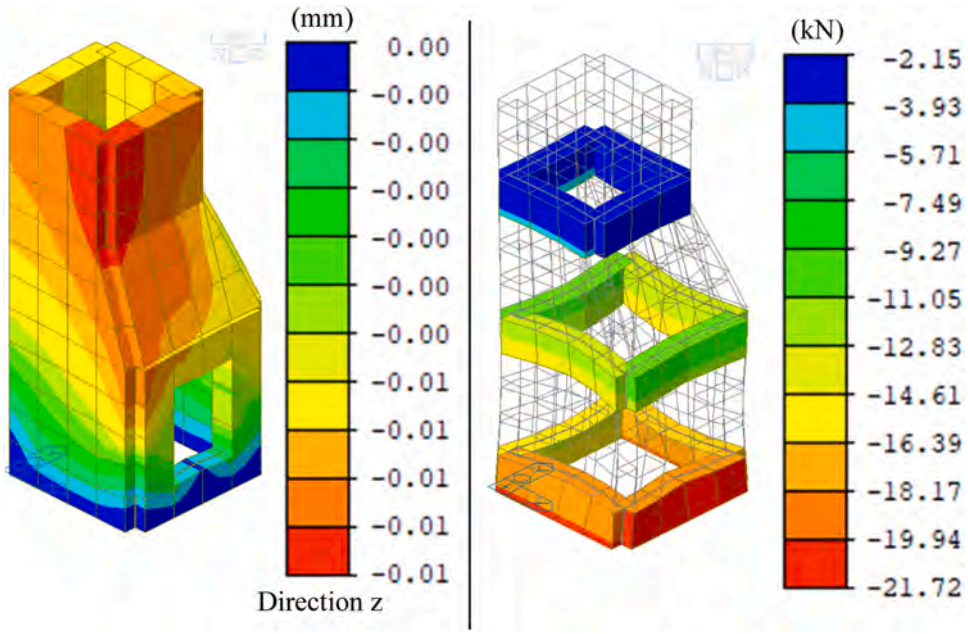

Fig. 16. Displacements and axial forces resulting from vertical loads for the Shaft 05.

3. Numerical Modeling

In the numerical modeling, the loads anticipated during the shafts' service life were considered. In static scenarios, the structure faced earth pressures at rest, while active earth pressures were applied during earthquakes. The structural elements experienced lateral

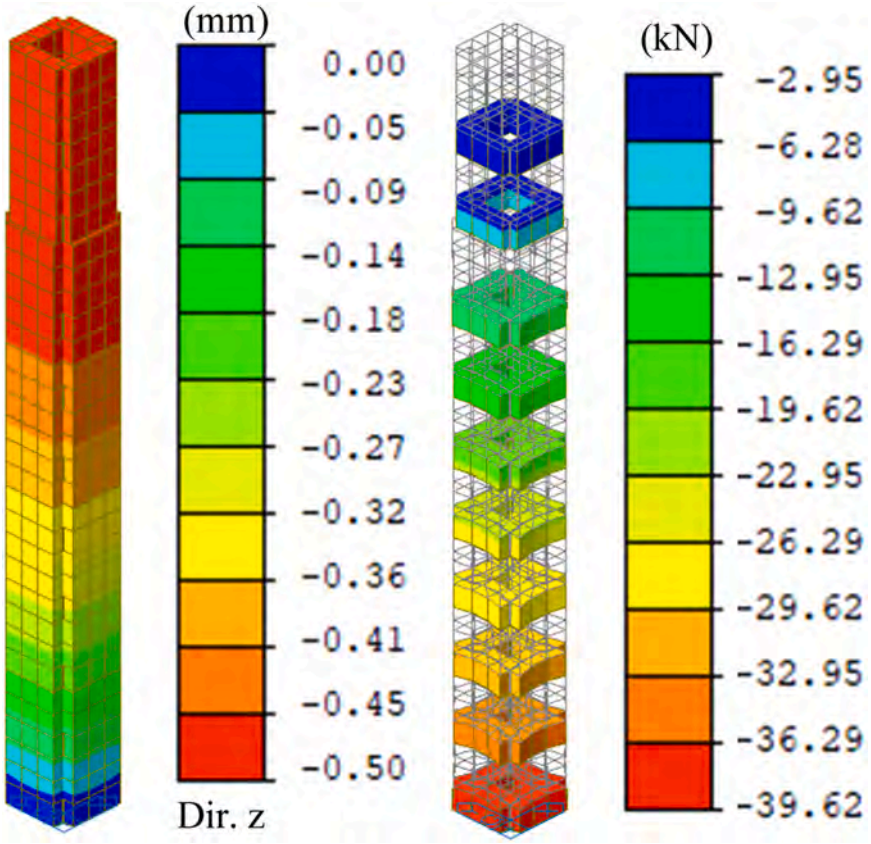

Fig. 17. Displacements and axial forces resulting from vertical loads for the Shaft 06.

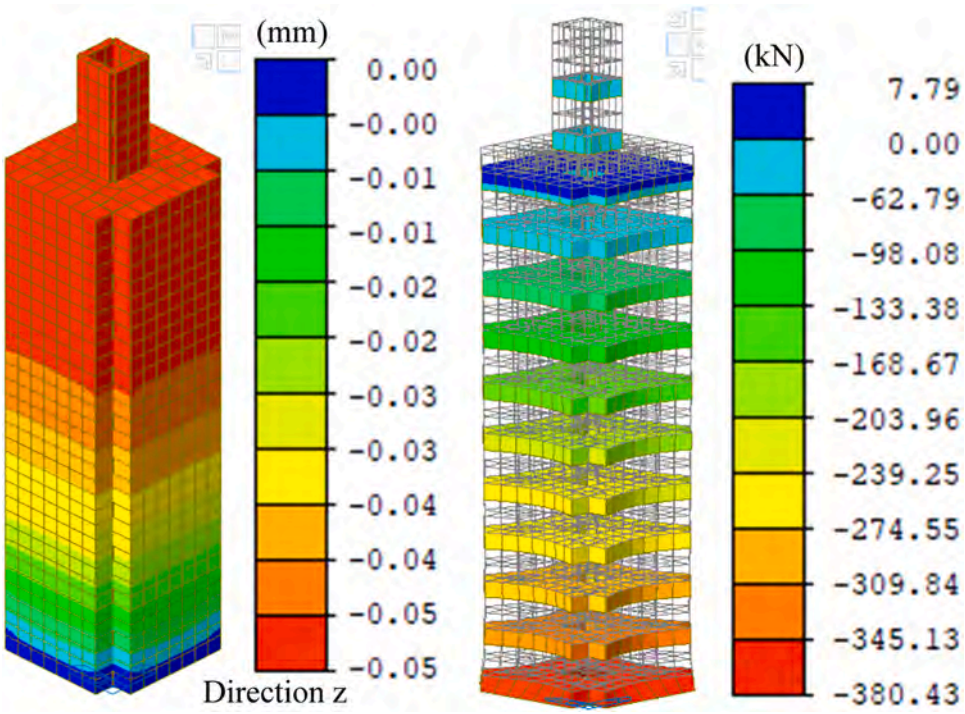

Fig. 18. Displacements and axial forces resulting from vertical loads for the Shaft 07.

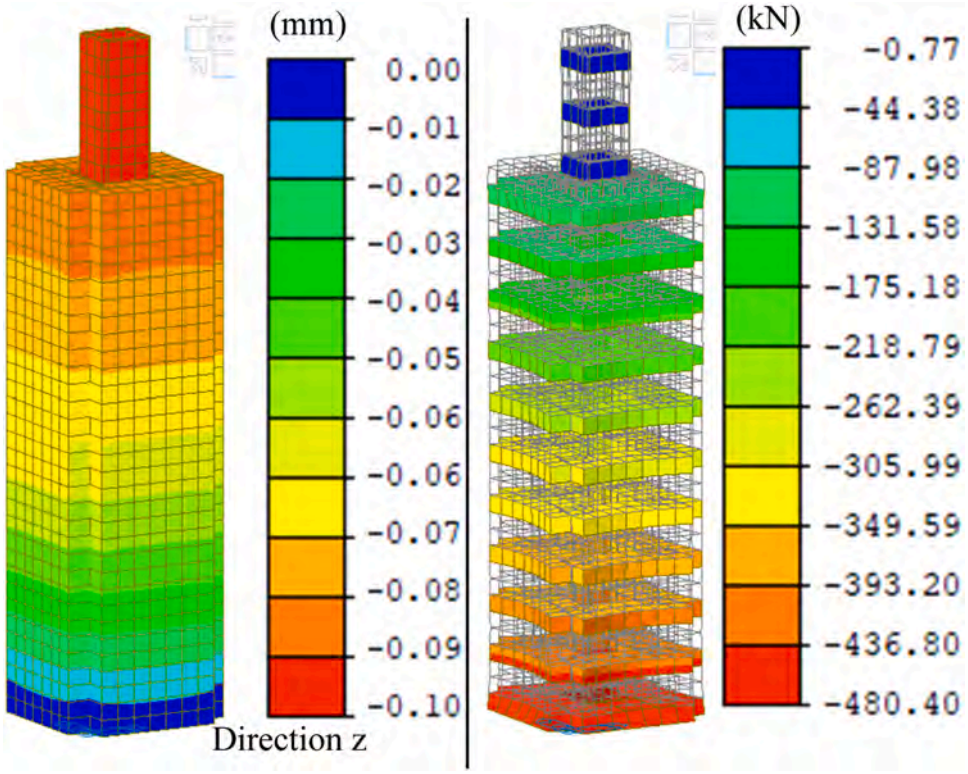

Fig. 19. Displacements and axial forces resulting from vertical loads for the Shaft 08.

loads due to surcharge loads based on their locations and placements. Additionally, groundwater induced lateral loads on the structural elements. Load combinations were determined according to criteria outlined in TBEC 2018 [23]. These load combinations applied to the models are detailed in Table 4. The structures endure vertical loads from the walls constituting the load-bearing system of the shaft, along with lateral pressures from the surrounding soil and surcharge. Furthermore, the structures face additional lateral loads due to seismic effects from the soil and surcharge. Figs. 3–6 illustrate the types of loading to which all shafts are subjected.

The structure models were created using Midas Gen [25], a finite element software, employing "plate/wall" elements. To simulate lateral behavior, nonlinear p-y springs were utilized to represent the interaction between the shaft surface and the ground. These p-y springs were modeled individually at each shaft node, oriented perpendicular to the shaft surface to transmit pressure only. The characteristics of the p-y springs were determined based on soil classes and calculated using the horizontal bedding coefficients specified in Table 2.

Considering the historical nature of the examined shafts, analysis methods were selected based on criteria outlined in applicable codes. Soil pressures were applied as specified in TBEC 2018. Loadings were adjusted according to the unit weight of soil, saturated unit weight of water, additional surcharge load, and water surface height. For the structural system and general behaviors of the shafts, "*Seismic Response Coefficient*" and "*Structure Importance Factor*" were taken as R=1 and I=1, respectively. The shafts were subjected to earthquake loads arising from their own weight, soil and surcharge pressures, as well as global soil displacement. The selected performance-based structural analysis and evaluation methods are detailed in Table 5. The target damage level for the analyzed structures is the controlled damage performance, which corresponds to damage that is not too severe and is mostly repairable to the structural system elements of the building, ensuring life safety. Nonlinear analysis was conducted using Midas software, since p-y springs function only under compression and do not accommodate tensile loads. The mesh size varied for each shaft but was around 250–300 mm.

The static effects considered include dead, permanent, and live loads, as well as soil pressure, soil loads, and temperature variations. These static effects were calculated specifically for shaft No. 1, with dead loads from the own weight of the structural elements applied as DC1 loading in the finite element model. Fig. 7 shows the variation of soil and surcharge pressures with depth under rest and active conditions.

Response spectra for DD-2 and DD-3 earthquake ground motions were generated (Fig. 8). Lateral earthquake forces were implemented as "Nodal Body Force" loading applied at the nodal points within the finite element model for the respective masses. The earthquake coefficients were defined according to Eq. 1 and Eq. 2 for DD-2 and DD-3 earthquake ground motions.

$$K_h = 0.4 \times 0.755 = 0.302 \quad (1)$$

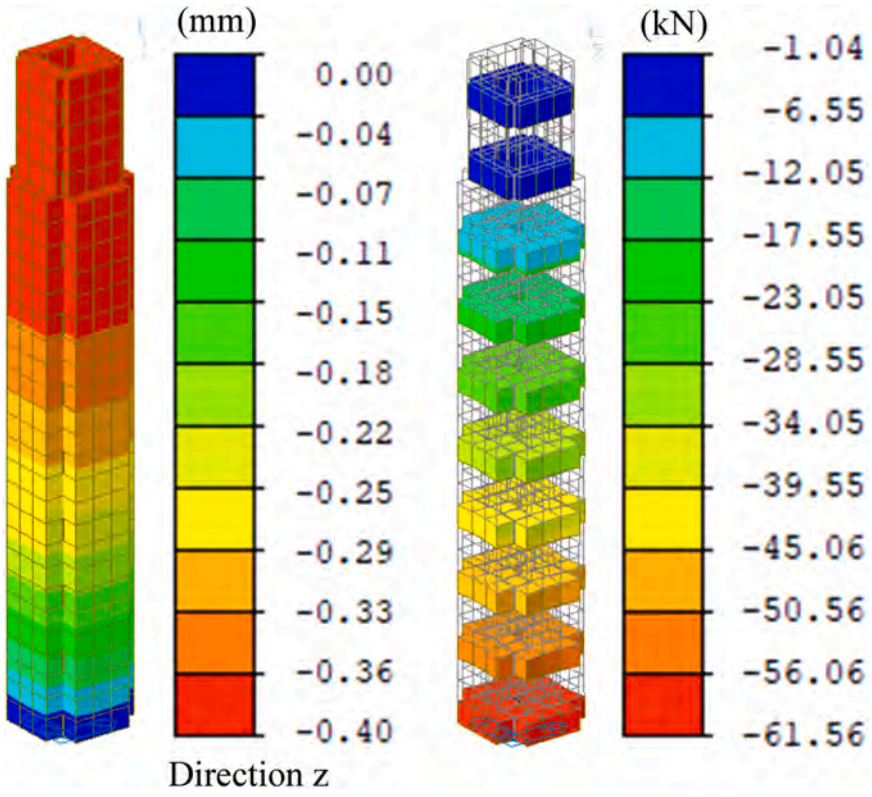

Fig. 20. Displacements and axial forces resulting from vertical loads for the Shaft 09.

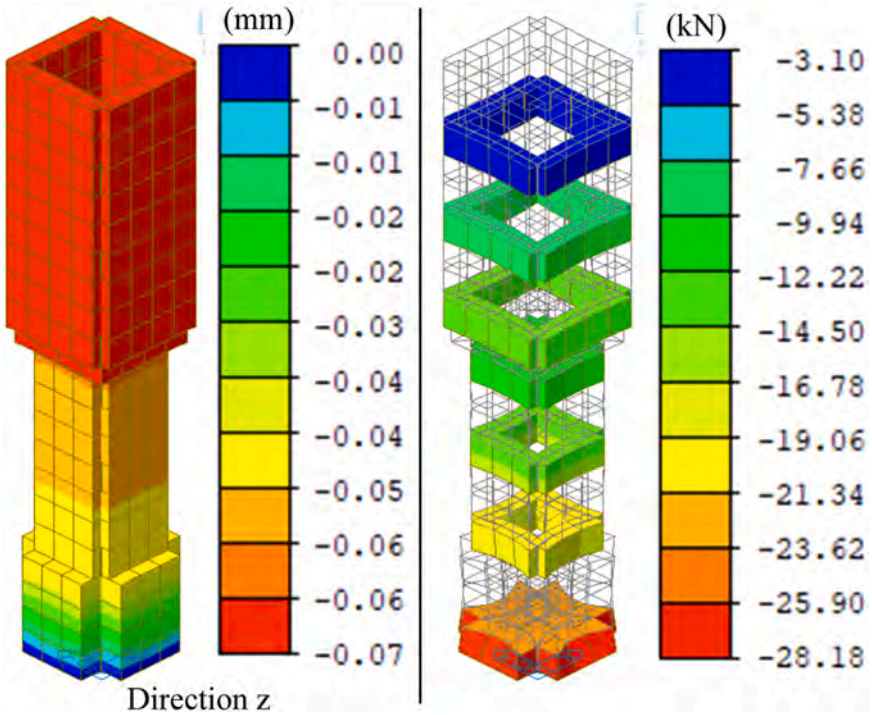

Fig. 21. Displacements and axial forces resulting from vertical loads for the Shaft 10.

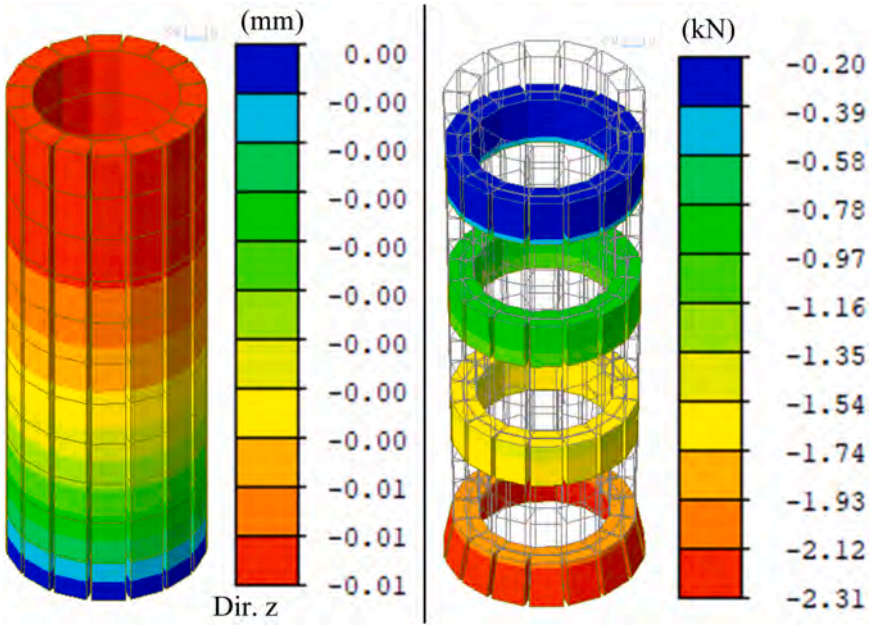

Fig. 22. Displacements and axial forces resulting from vertical loads for the Shaft 11.

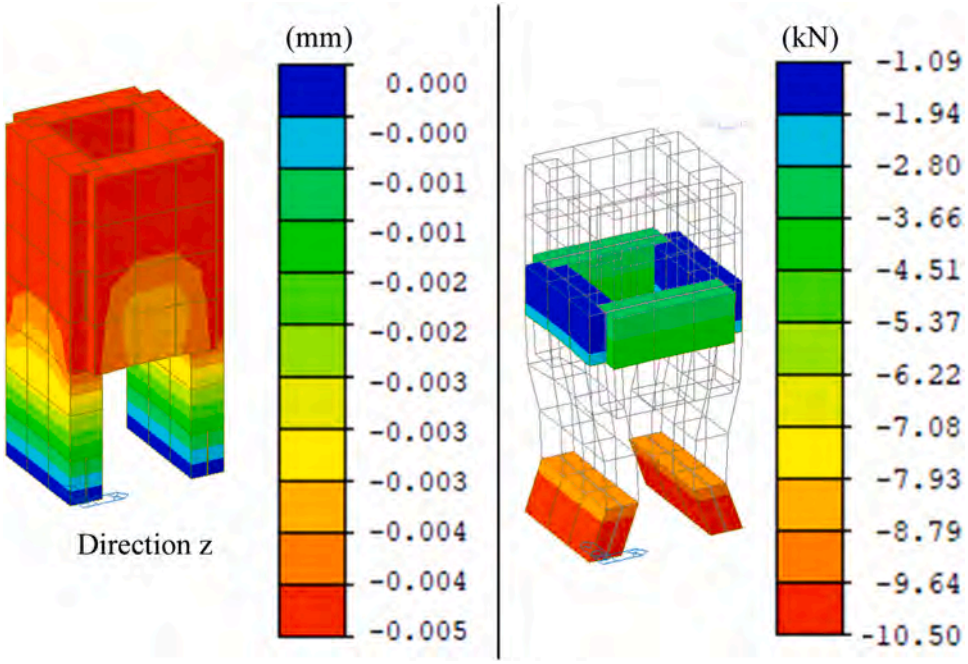

Fig. 23. Displacements and axial forces resulting from vertical loads for the Shaft 12.

$$K_h = \quad 0.4 \quad \times \quad 0.303 \quad = 0.121 \tag{2}$$

Fig. 9 illustrates the variation of soil pressures with depth, calculated for earthquake effects caused by soil loads. Fig. 10 depicts the variation of surcharge pressures with depth, calculated for earthquake effects resulting from a surcharge load of 10 kN/m^2. The 3-D finite element model of the shafts is presented in Fig. 11.

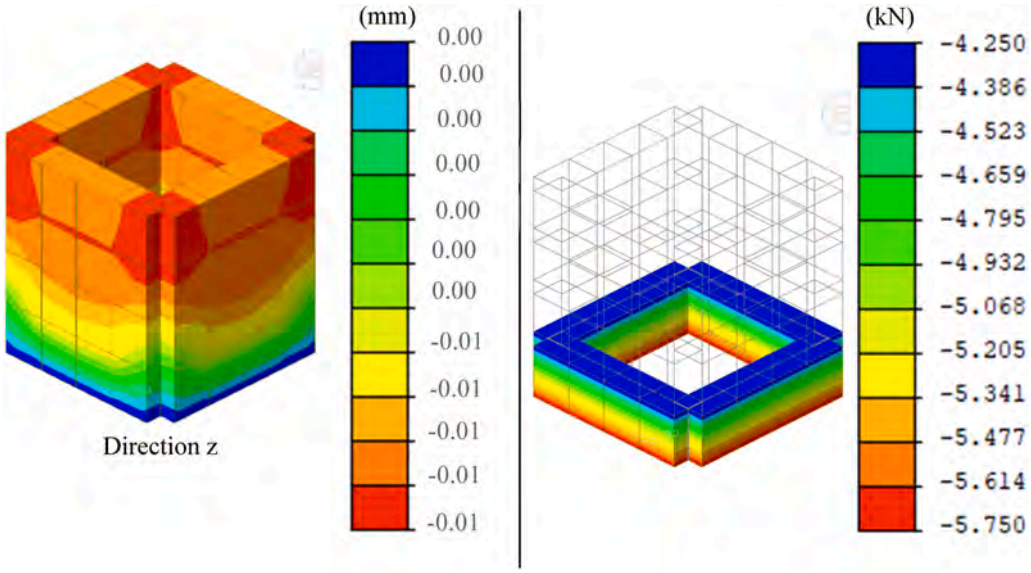

Fig. 24. Displacements and axial forces resulting from vertical loads for the Shaft 13.

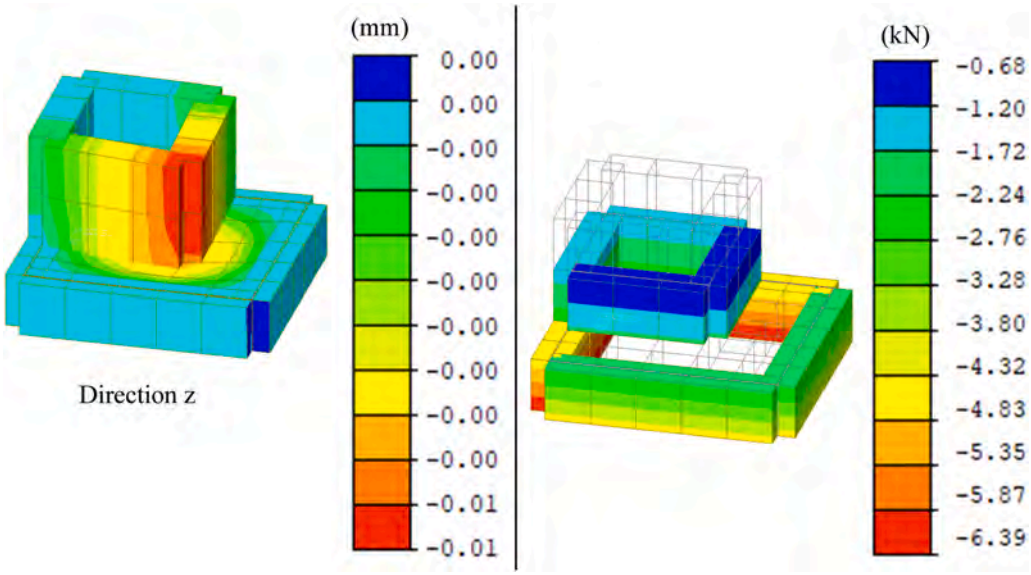

Fig. 25. Displacements and axial forces resulting from vertical loads for the Shaft 14.

4. Analysis results

Figs. 12–26 illustrate displacements and axial forces on the shafts under vertical loads. The compressive stresses induced by these forces on the masonry walls were compared against allowable stresses specific to the corresponding masonry wall type to ensure they did not exceed specified limits. Additionally, Figs. 27 to 41 show lateral displacements and shear forces resulting from DD-2 and DD-3 earthquake ground motions in the x and y directions, respectively. A strength-based assessment was conducted for the shaft walls in accordance with the ERMGHB 2017 local code. According to this code, the average stresses are calculated using axial and shear force values, which are then compared with the limit values. Therefore, the axial force and shear force values needed to calculate the average stresses are presented instead of the stress distribution in the walls along the shaft height.

Analysis results for the examined shafts and performance assessments for DD-2 and DD-3 earthquake ground motions are summarized in Table 6. The "Limit (%) ERMGHB" column in the table indicates the ratio of shear force acting on the walls failed in shear to the total shear force on the same story. As an important part of the presented methodology, all shafts examined were segmented at regular intervals, with each segment defined as a separate story. In the Midas model, each element forming the shaft was defined as a

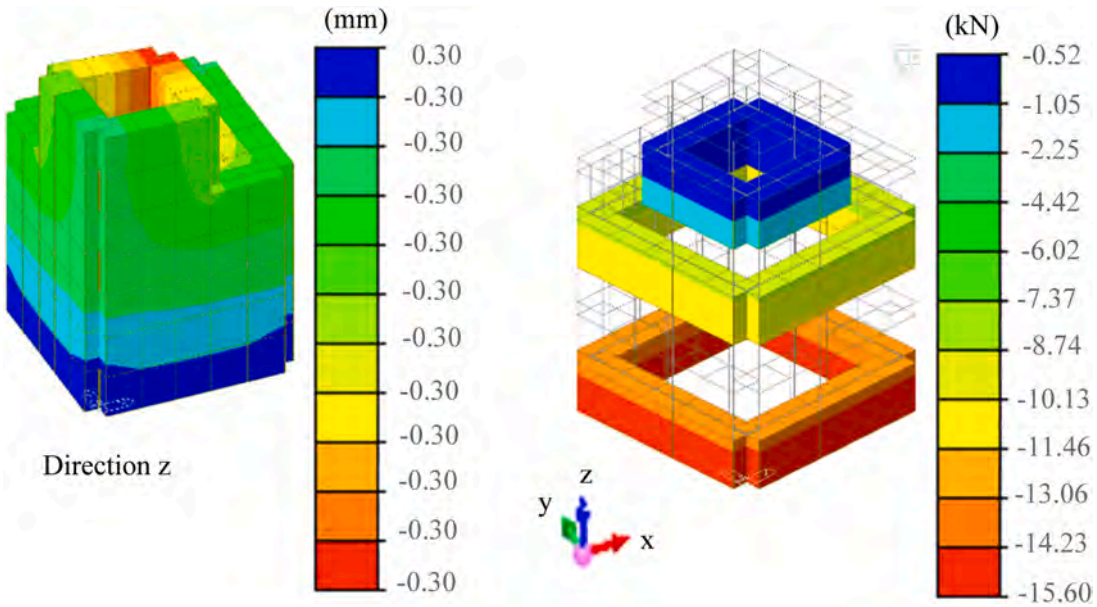

Fig. 26. Displacements and axial forces resulting from vertical loads for the Shaft 15.

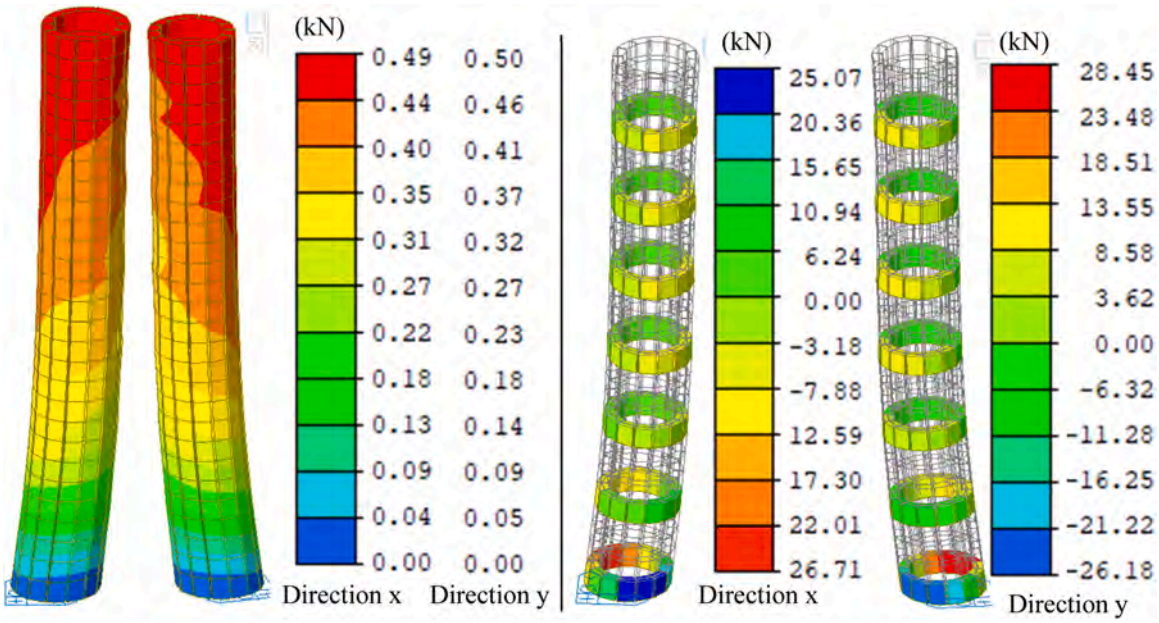

Fig. 27. Lateral displacements and shear forces resulting from earthquake effects for the Shaft 01.

'six-degree-of-freedom 6DOF PLATE'. To represent the effects along the shaft height, the plate elements at certain elevations are defined as walls/segments. Consequently, no separate transition element is used between the segments in the numeric models.

5. Conclusion and remarks

This study presents a methodology for the numerical seismic assessment of the shafts of the *Atik Valide* Waterway. The key findings obtained from the analyses are summarized as follows:

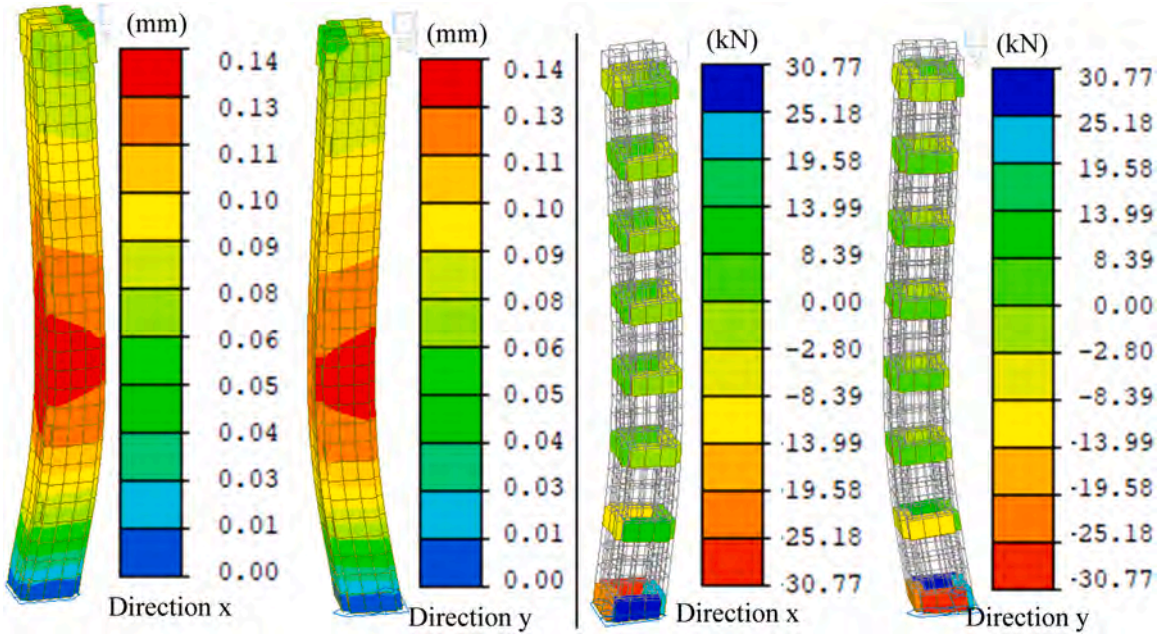

Fig. 28. Lateral displacements and shear forces resulting from earthquake effects for Shaft 02 (DD-2).

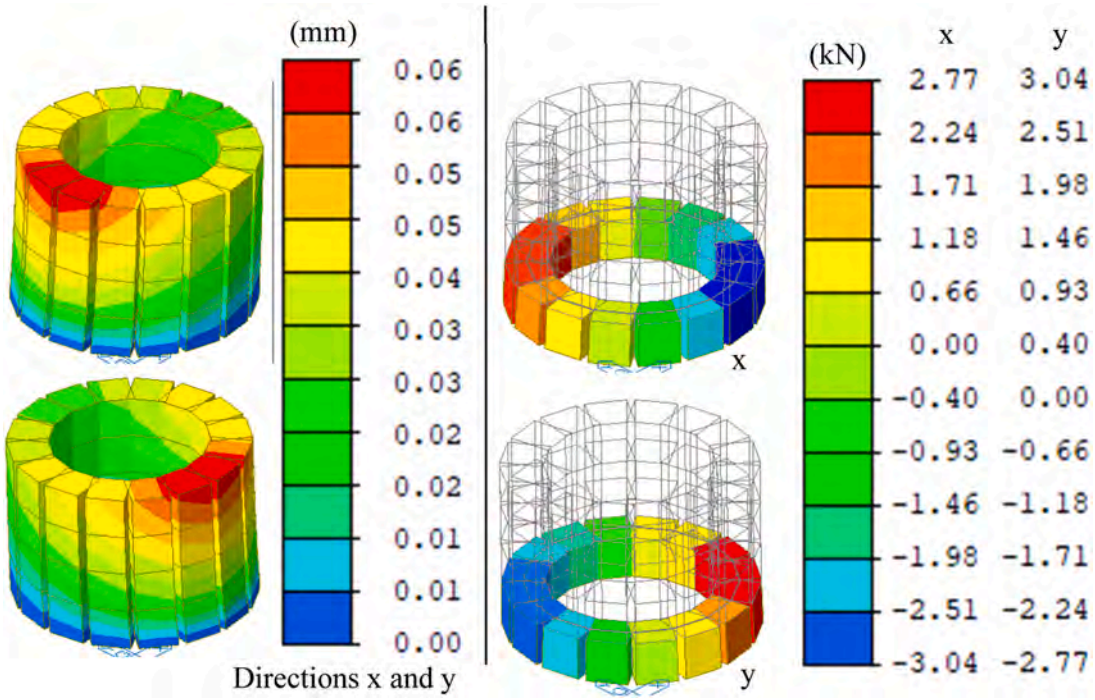

Fig. 29. Lateral displacements and shear forces resulting from earthquake effects for Shaft 03 (DD-2).

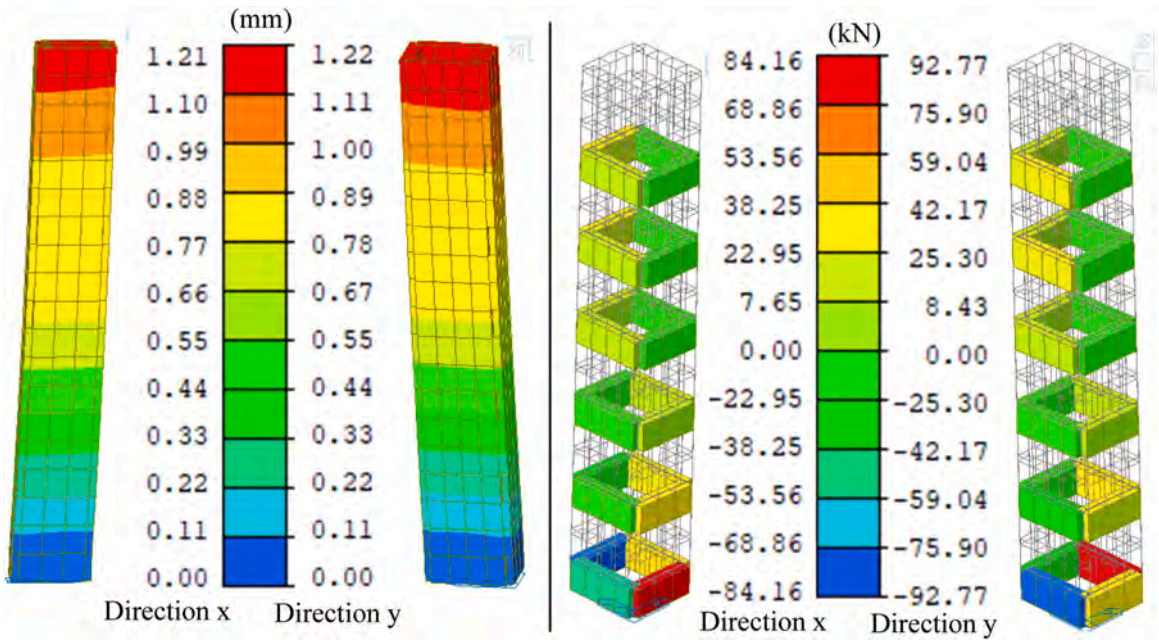

Fig. 30. Lateral displacements and shear forces resulting from earthquake effects for Shaft 04 (DD-2).

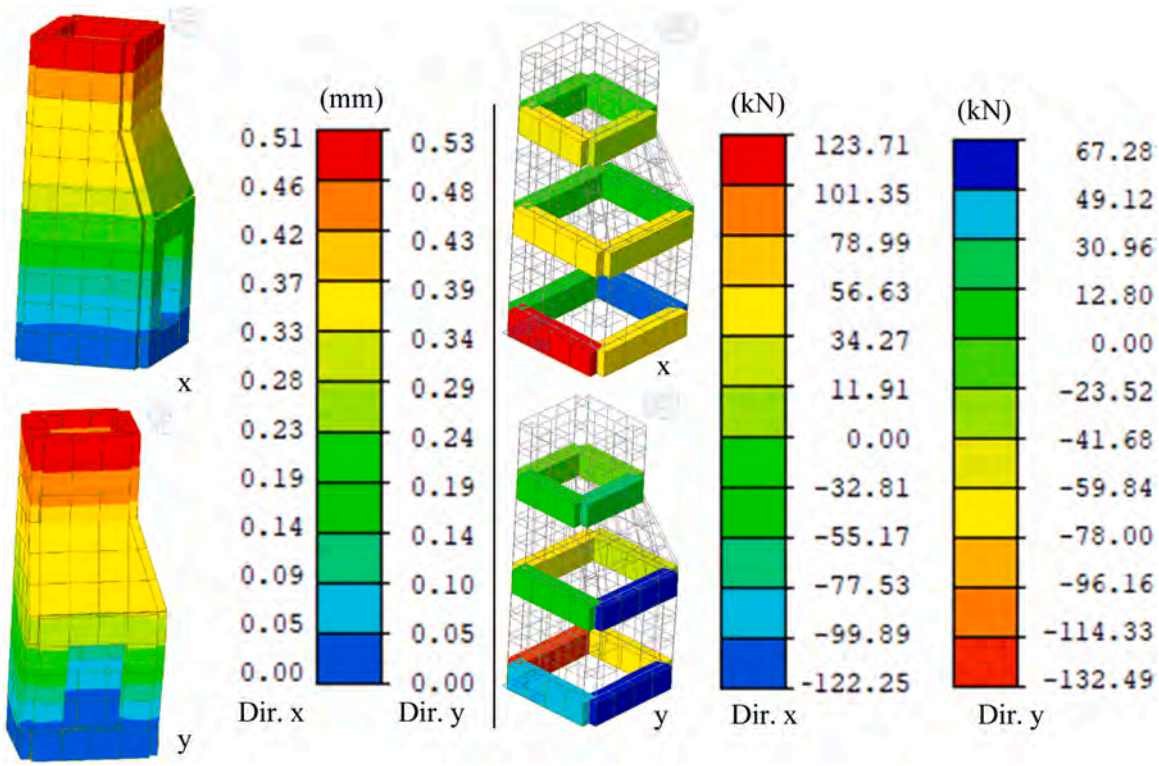

Fig. 31. Lateral displacements and shear forces resulting from earthquake effects for Shaft 05 (DD-2).

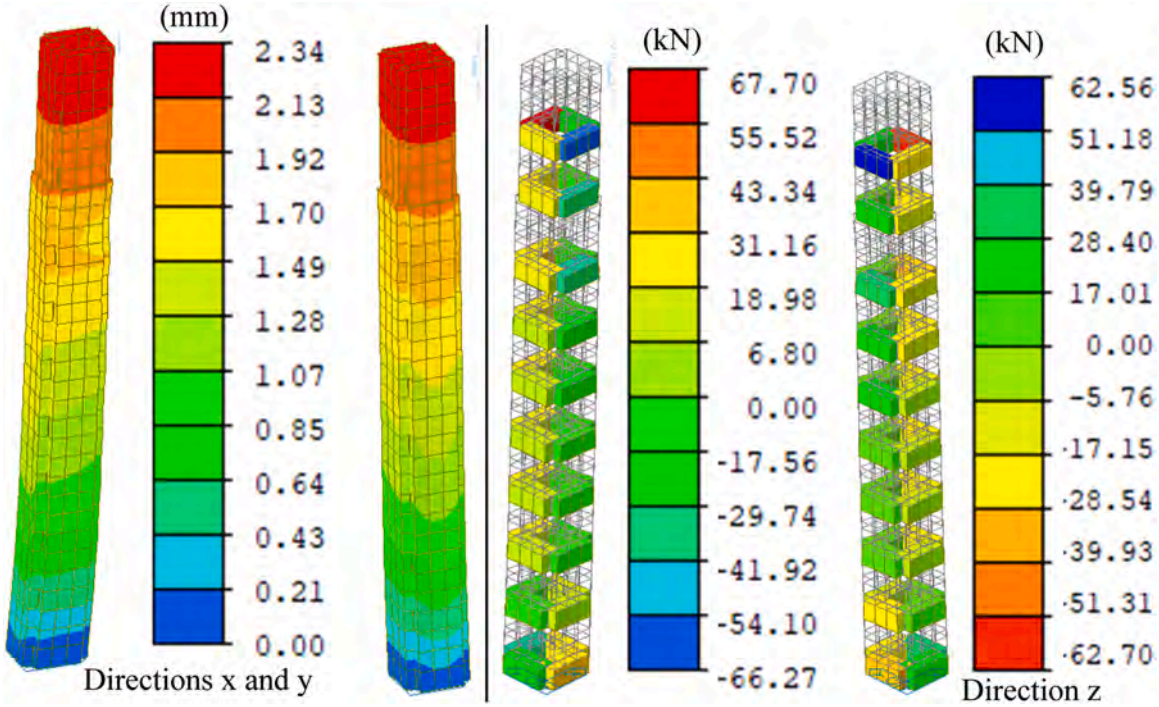

Fig. 32. Lateral displacements and shear forces resulting from earthquake effects for Shaft 06 (DD-2).

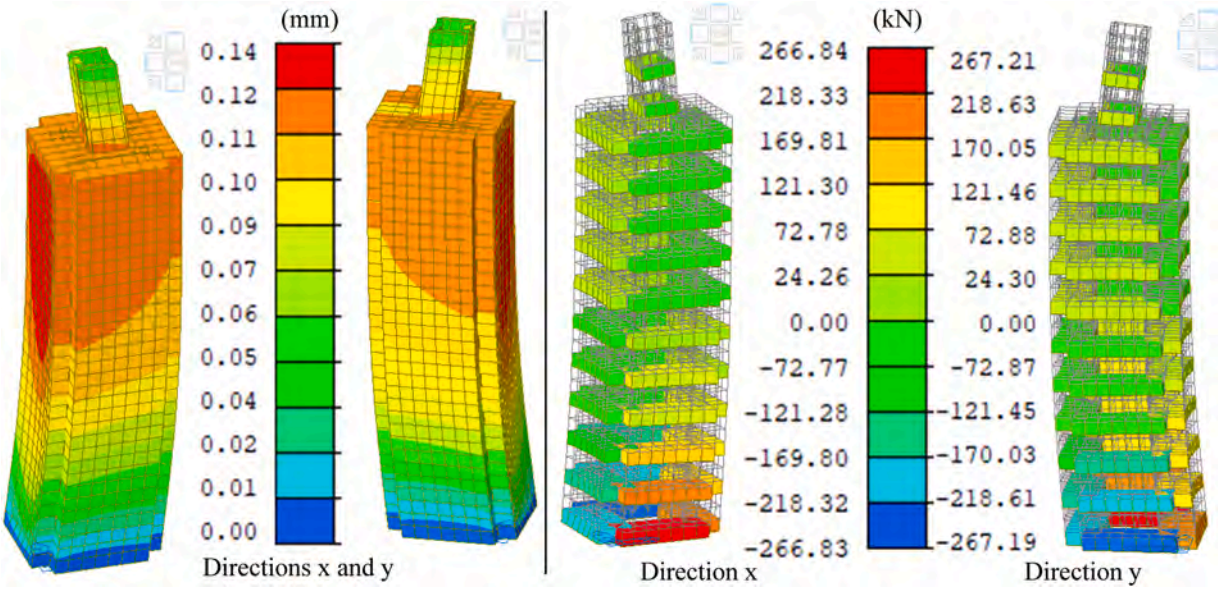

Fig. 33. Lateral displacements and shear forces resulting from earthquake effects for Shaft 07 (DD-2).

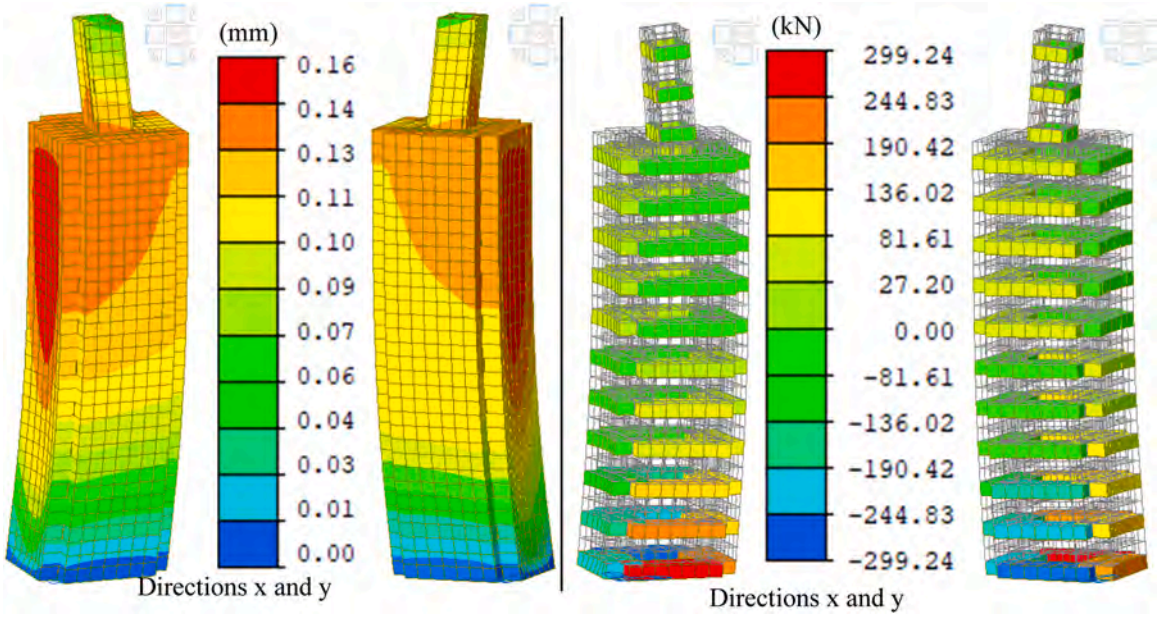

Fig. 34. Lateral displacements and shear forces resulting from earthquake effects for Shaft 08 (DD-2).

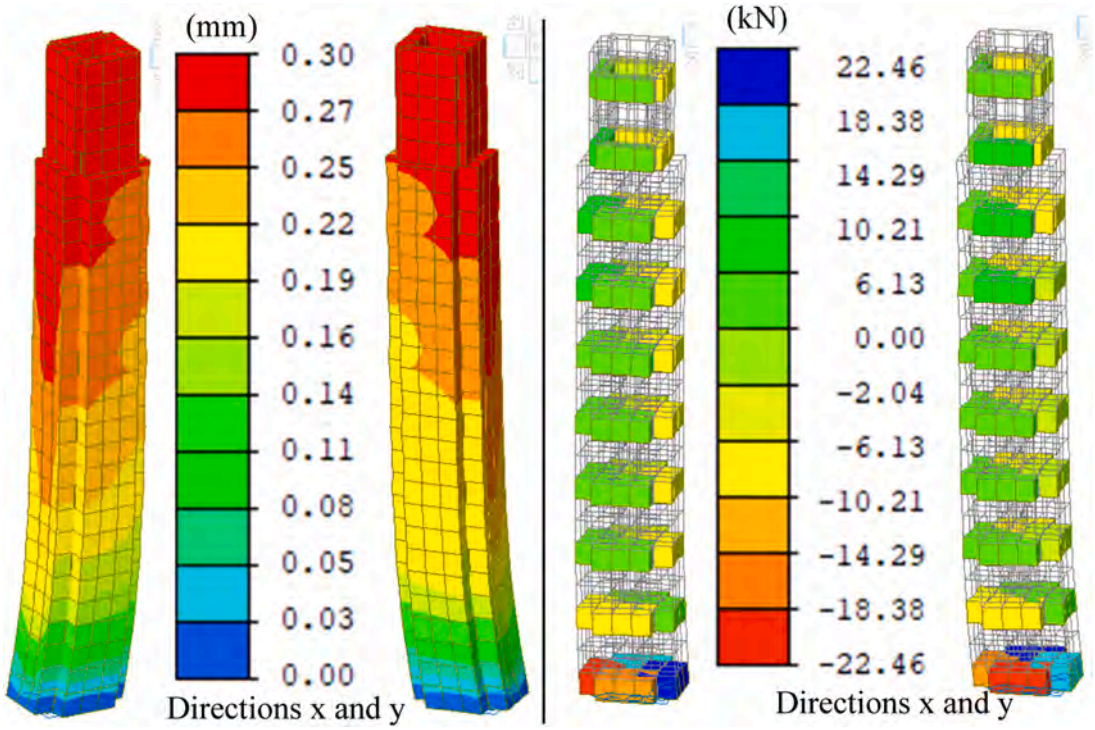

Fig. 35. Lateral displacements and shear forces resulting from earthquake effects for Shaft 09 (DD-2).

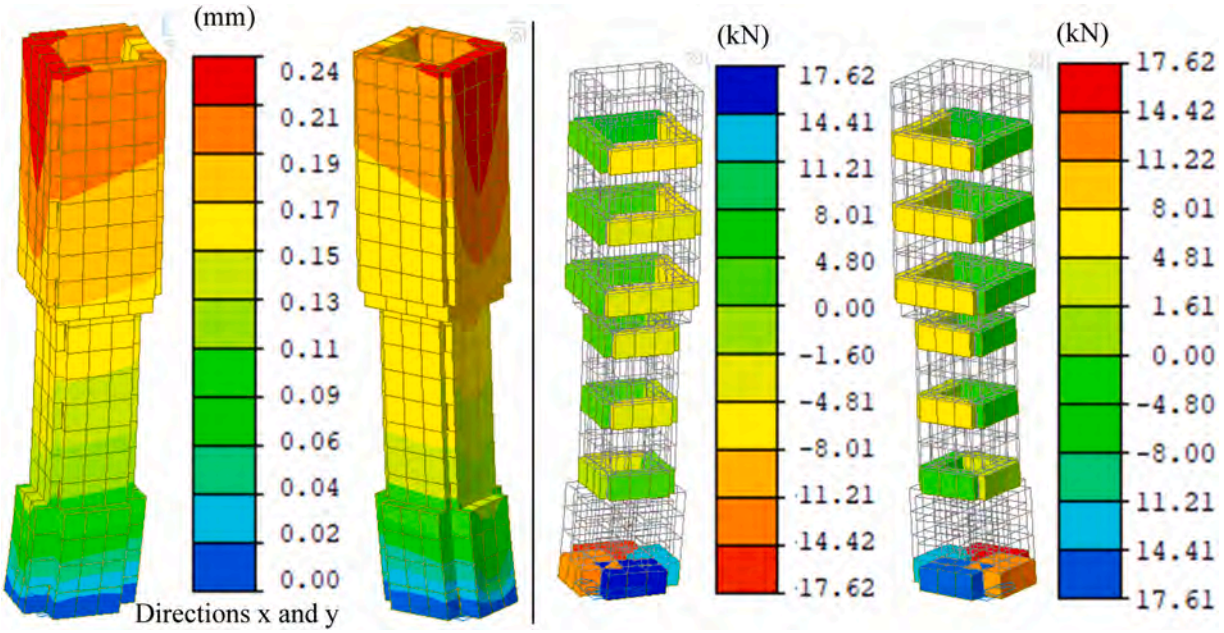

Fig. 36. Lateral displacements and shear forces resulting from earthquake effects for Shaft 10 (DD-2).

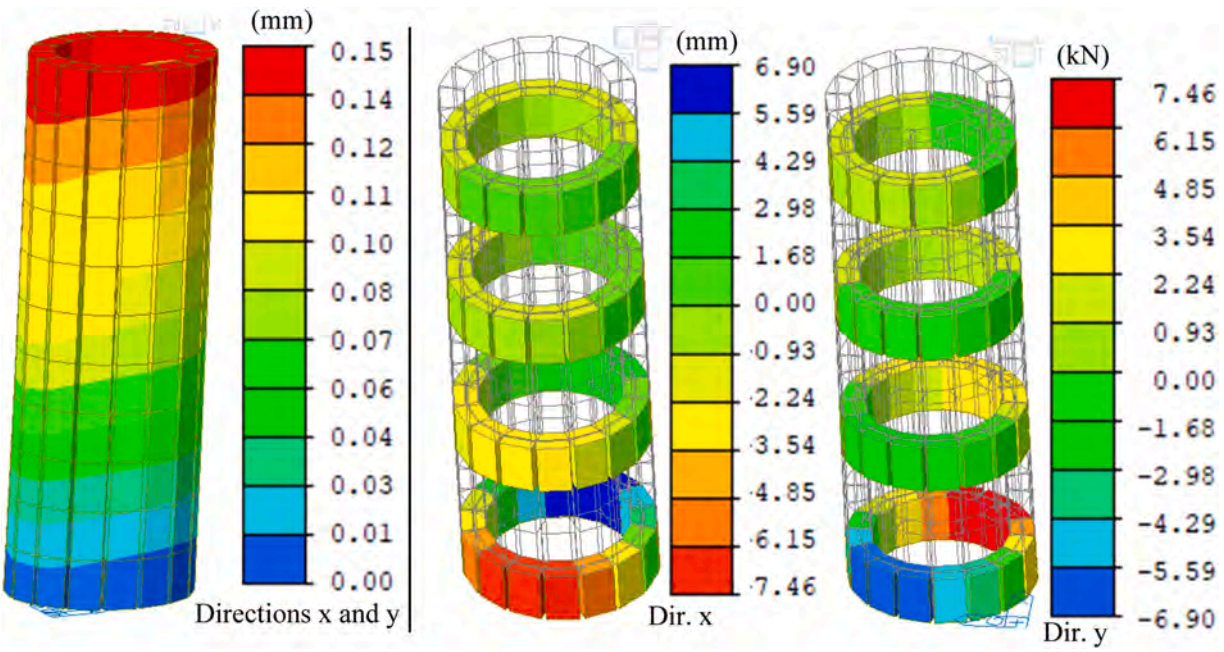

Fig. 37. Lateral displacements and shear forces resulting from earthquake effects for Shaft 11 (DD-2).

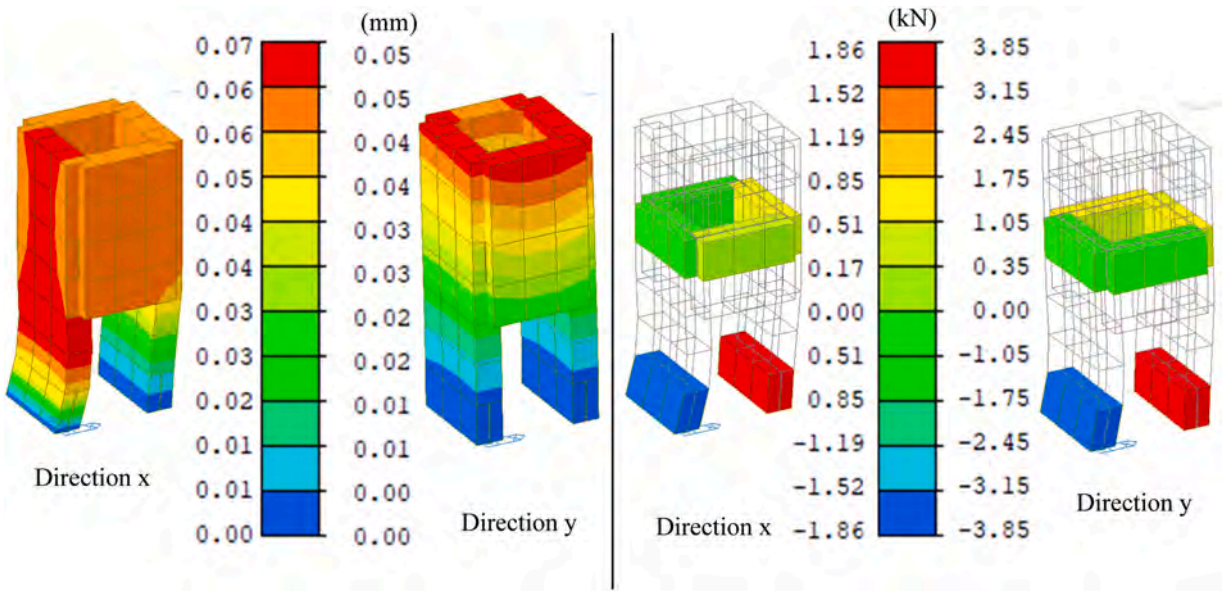

Fig. 38. Lateral displacements and shear forces resulting from earthquake effects for Shaft 12 (DD-2).

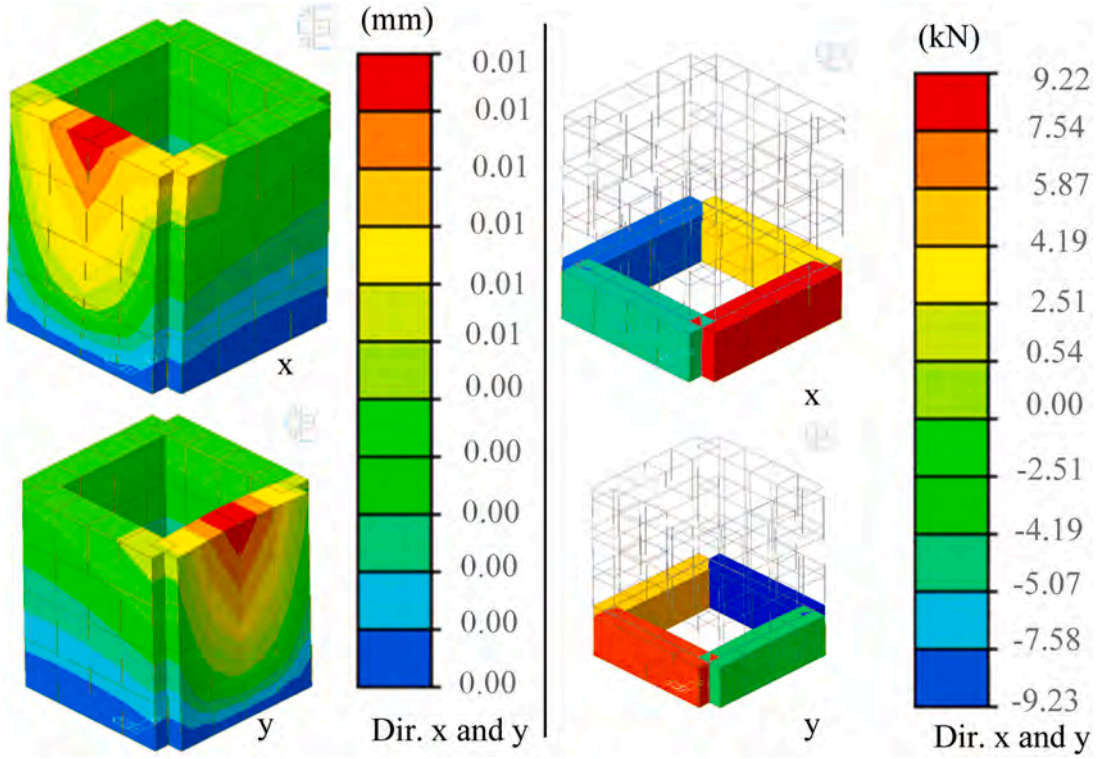

Fig. 39. Lateral displacements and shear forces resulting from earthquake effects for Shaft 13 (DD-2).

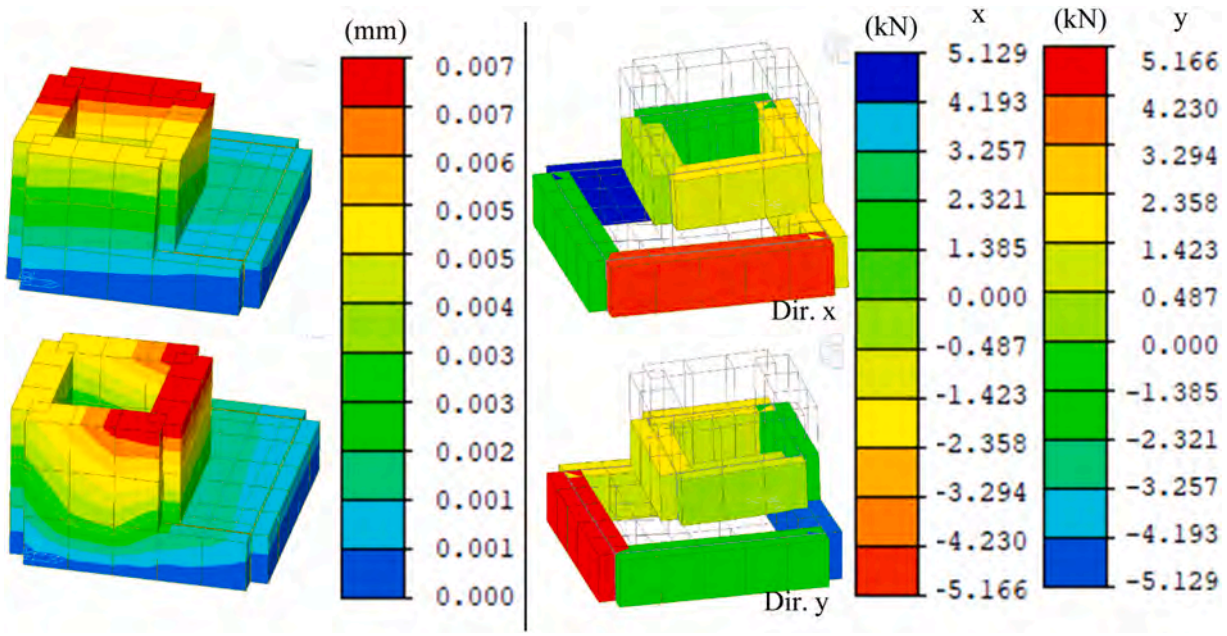

Fig. 40. Lateral displacements and shear forces resulting from earthquake effects for Shaft 14 (DD-2).

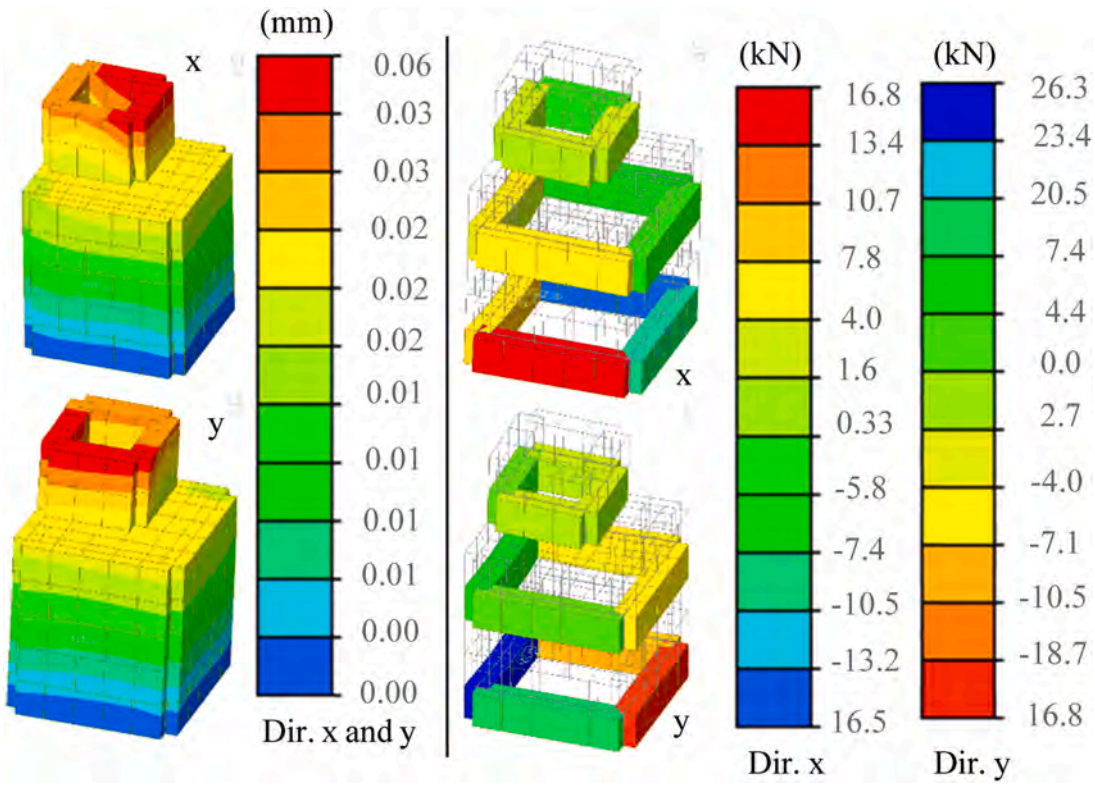

Fig. 41. Lateral displacements and shear forces resulting from earthquake effects for Shaft 15 (DD-2).

Table 6
Performance analysis results of the shafts.

Shaft no	Shear Failure Ratio (%)[a,b]		Limit (%) ERMGHB [24]		Check (√ / ×)	
	DD−3	**DD−2**	**DD−3**	**DD−2**	**DD−3**	**DD−2**
1	13.09	64.27	40		√	×
2	–	–	40		√	√
3	–	–	40		√	√
4	–	100.00	40		√	×
5	–	65.14	40		√	×
6	–	–	40		√	√
7	–	–	40		√	√
8	–	–	40		√	√
9	–	–	40		√	√
10	–	–	40		√	√
11	–	–	40		√	√
12	–	–	40		√	√
13	–	–	40		√	√
14	–	–	40		√	√
15	–	–	40		√	√

[a] During the evaluation of whether the target performance level was achieved, shear force checks were considered.
[b] The most unfavorable situation among the four earthquake directions was considered for each floor.

Table 7
“The "Controlled Damage" target performance assessments for all shafts.

Earthquake ground motion level	01	02	03	04	05	06	07	08	09	10	11	12	13	14	15
DD−3	√	√	√	√	√	√	√	√	√	√	√	√	√	√	√
DD−2	×	√	√	×	×	√	√	√	√	√	√	√	√	√	√

- For all shafts, the axial forces applied on the vertical load-bearing elements due to static effects (dead load, horizontal soil load, and surcharge load) were determined to be smaller than the axial strength of these elements. As a result, the shafts meet the axial strength criteria specified in the applicable codes.
- The analysis results indicate that all shafts meet the “Controlled Damage” target performance for a DD-3 earthquake with a 50 % probability of exceedance in 50 years (recurrence period 72 years).
- Except for shafts 1, 4, and 5, all other shafts were found to satisfy the “Controlled Damage” target performance for a DD-2 ground motion with a 10 % probability of exceedance in 50 years (recurrence period 475 years).
- It can be argued that the numerical modeling results align with the observed conditions of the shafts, demonstrating that the modeling methodology is a consistent and reliable approach to the numerical representation of such underground structures.

The "Controlled Damage" target performance assessments of the shafts for DD-2 and DD-3 earthquake ground motions, based on criteria outlined in the code, are presented in Table 7.

In conclusion, the numerical analyses revealed that overall, these shaft structures, although constructed about 400 years ago, meet the current seismic demands specified in the codes. The unique methodology followed in this study yielded reliable outcomes. The authors believe that this study can serve as a reference for similar work and studies aimed at determining the seismic performance of similar underground structures.

CRediT authorship contribution statement

turhan bilir: Visualization, Supervision. **onur şimşek:** Investigation, Data curation. **karsu hatipoğlu:** Resources, Methodology. **Baris Sayin:** Writing – review & editing, Methodology. **barış gunes:** Software. **turgay cosgun:** Data curation. **namık aysal:** Formal analysis. **kamran samadi:** Writing – original draft, Investigation.

Declaration of Competing Interest

The authors declare that they have no known competing financial interests or personal relationships that could have appeared to influence the work reported in this paper.

Acknowledgments

This study was conducted as part of the "Determination of Underground and Aboveground Structures of Historical Waterways Project (Grand ID: 2022/32, Istanbul, Türkiye)" undertaken by Istanbul University-Cerrahpaşa, Project and Tecnology Office

(PROTEK) and Istanbul Water and Sewerage Administration General Directorate. Project coordinators are Prof. Dr. Namık Aysal and Dr. Onur Şimşek.

Data Availability

No data was used for the research described in the article.

References

[1] M. Uçar, Gaziantep historical water system and water structures, METU, J. Fac. Archit. 2 (2016) 73–100.
[2] K. Çeçen, The peak of Ottoman Empire 16th century technology (in), İSKİ Press, Turkish, 2000.
[3] Y. Sağır, "Ottomanese water foundations". The pursuit of history, Int. Period. Hist. Soc. Res. 15 (2016) 445–473.
[4] Çeçen, K., 1988. Mimar Sinan and Kırkçeşme facilities. İSKİ Press.
[5] Ş. Sönmezer, S. Şahin, İ.K. Kolay, Ottoman period waterway structures in Istanbul, Turk. Stud. 13 (2018) 1191–1226.
[6] K.Y. Kim, D.S. Lee, J. Cho, S.S. Jeong, S. Lee, The effect of arching pressure on a vertical circular shaft, Tunn. Undergr. Space Technol. 37 (2013) 10–21.
[7] Z. Chen, B. Zhang, Seismic responses of the large-scale deep shaft in shanghai soft soils, Adv. Soil Dyn. Found. Eng. (2018) 103–111.
[8] N.E. Faustin, M.Z.E.B. Elshafie, R.J. Mair, Centrifuge modelling of shaft excavations in clay, April 2017. *9th International Symposium on Geotechnical Aspects of Underground Construction in Soft Ground*, Taylor & Francis Group, Sao Paulo, London, 2018.
[9] Z. Chena, P. Jia, Three-dimensional analysis of effects of ground loss on static and seismic response of shafts, Tunn. Undergr. Space Technol. 92 (2019).
[10] B. Zhanga, Z. Chen, Effects of nominal flexibility ratio and shaft dimensionless parameters on the seismic response characteristics of deep shafts, Soil Dyn. Earthq. Eng. 120 (2019) 257–261.
[11] J. Zhanga, Y. Yuanc, E. Bilottab, B. Zhanga, H. Yu, Analytical solution for dynamic responses of the vertical shaft in a shaft-tunnel junction under transverse loads, Soil Dyn. Earthq. Eng. 126 (2019).
[12] S.Y. Kwon, M. Yoo, A study on the dynamic behavior of a vertical tunnel shaft embedded in liquefiable ground during earthquakes, Appl. Sci.: Spec. Issue Adv. Methods Seism. Perform. Eval. Build. Struct. II 11 (2021).
[13] B. Zhang, L. Lu, Z. Zhong, X. Du, M.H.E. Naggar, Analytical solution for seismic response of vertical shaft with primary and secondary linings under sh wave excitation, Comput. Geotech. 164 (2023).
[14] Z. Li, J. Lai, Z. Ren, Y. Shi, X. Kong, Failure mechanical behaviors and prevention methods of shaft lining in China, Eng. Fail. Anal. 143 (2023).
[15] K.-Y. Kim, D.-S. Lee, J. Cho, S.-S. Jeong, S. Lee, The effect of arching pressure on a vertical circular shaft, Tunn. Undergr. Space Technol. 37 (2013) 10–21.
[16] Y. Qiao, F. Xie, Z. Bai, J. Lu, W. Ding, Deformation characteristics of ultra-deep circular shaft in soft soil: a case study, Undergr. Space (2024) 239–260.
[17] A. Chehadeh, A. Turan, F. Abed, M. Yamin, Lateral earth pressures acting on circular shafts considering soil-structure interaction, Int. J. Geotech. Eng. (2017) 1–15.
[18] E. Mahmoodi, P. Malekzadeh, S.R. Mohebpour, Dynamic torsional analysis of a functionally graded coated circular shafts weakened by multiple radial cracks, Theor. Appl. Fract. Mech. 121 (2022) 1–14.
[19] J. Cho, H. Lim, S. Jeong, K. Kim, Analysis of lateral earth pressure on a vertical circular shaft considering the 3D arching effect, Tunn. Undergr. Space Technol. 48 (2015) 11–19.
[20] A. Chehadeh, A. Turan, F. Abed, Numerical investigation of spatial aspects of soil structure interaction for secant pile wall circular shafts, Comput. Geotech. 69 (2015) 452–461.
[21] ERMGHB 2017 Earthquake Risk Management Guide for Historical Buildings, General Directorate of Foundations.
[22] TTEC 2020, Turkish Highways and Railways Tunnels and Other Ground Structures Earthquake Code, Ministry of Transport and Infrastructure, Republic of Turkey, Official Gazette, 06.10.2020, 31266 (in Turkish).
[23] TBEC 2018 Turkey Building Seismic Code: Rules for design of buildings under earthquake effect, Official Gazette, 18.03.2018, 30364 (in Turkish).
[24] ASCE/SEI 7-16 Minimum Design Loads and Associated Criteria for Buildings and Other Structures, American Society of Civil Engineers, Virginia.
[25] Midas Gen (2018), Integrated Solution System for Building and General Structures, MIDAS Information Technology Co.